Low-Frequency Sound Propagation in the Yellow Sea

Results from the 1996 China-U.S. Experiment

by P.H. Dahl, C.J. Eggen, D.J. Tang, and R.C. Spindel

Technical Report
APL-UW TR 9804
December 1998

Applied Physics Laboratory   University of Washington
1013 NE 40th Street   Seattle, Washington 98105-6698

1998123/ 114

ACKNOWLEDGMENTS

ABSTRACT

Two sets of acoustic measurements made by the Applied Physics Laboratory, University of Washington, as part of the August 1996 joint U.S.–China Yellow Sea Experiment are analyzed. One set consists of broadband propagation measurements for which explosive TNT sources were used. These data were reduced to estimates of calibrated transmission loss, which, along with the recorded signal waveforms, were interpreted to infer a geoacoustic model for the seabed. The other set consists of narrowband acoustic fluctuation measurements plus broadband ambient noise measurements. The data show an extraordinary time history during which the ambient noise level varies by as much as 30 dB over a period of 6 to 7 hours.

CONTENTS

LIST OF FIGURES

LIST OF TABLES

EXECUTIVE SUMMARY

This report presents results of a project to process and analyze acoustic measurements taken by the Applied Physics Laboratory at the University of Washington (APL-UW) during the joint U.S.–China Yellow Sea Experiment conducted 21–31 August 1996 near the approximate geographic center of the Yellow Sea (37°N, 124°E) in waters approximately 75 m deep.

Two sets of measurements are discussed. One set consists of broadband acoustic propagation measurements, for which sound sources (TNT explosive charges) were deployed at ranges from 0.7 km to 37 km and signals were received on a 16-element vertical line array deployed over the side of the primary research vessel, *Shi Yan 3*. These measurements were converted to calibrated estimates of acoustic transmission loss (TL)) in third-octave bands. The TL estimates were interpreted, together with the signal waveforms, in order to infer a geoacoustic model for the seabed representing this area of the Yellow Sea. We view the geoacoustic model as provisional; further analysis (see below) may lead to some modification.

The geoacoustic model consists of a 2-m-thick sediment with a sound speed of 1555 m/s and an attenuation of 0.2 dB/λ, where λ is the acoustic wavelength. This layer separates the water from a basement halfspace for which the sound speed is 1700 m/s and the attenuation is 0.07 dB/λ. Our measurements are not sensitive to density, and we assume the layer and halfspace densities are 1.5 g/cm^3 and 1.7 g/cm^3, respectively. The geoacoustic model applies to the nominal frequency range 100–1000 Hz.

We also determined from the recorded waveforms that the preset detonation depth for TNT charges (50 m) was off by 10 m on average, and we included this effect in our estimation of transmission loss.

The second set of measurements consists of narrowband acoustic fluctuation measurements and broadband ambient noise measurements made with a four-element vertical array deployed approximately 4 km east of the *Shi Yan 3*, which recorded acoustic data continuously for 38 hours. Two of the recording channels failed, but the remaining two recorded an extraordinary time history during which the ambient noise level varied by as much as 30 dB over a period between 6 and 7 hours. This period appears to be associated with the M2, or principal lunar, tidal mode (being roughly half the M2 period). A 290-Hz cw tone was emitted from a source suspended from the *Shi Yan 3* for 12 of the 38 hours; the subsequent recordings yielded valuable information on the nature of intensity fluctuations in the Yellow Sea. Temperature was also recorded on this mooring at three locations separated vertically. Spectra of both the intensity and temperature fluctuations assume a similar power-law decay of frequency to the minus 2.5 power.

Further analysis to be carried out by APL-UW is recommended, and research along the following lines of inquiry will pay off in terms of understanding the nature of acoustic propagation in the Yellow Sea:

1. On the significance (if any) of the vertical variation seen in our transmission loss estimates.

2. On the energy spectrum of the so-called headwaves observed in the data, particularly the spectral peak and bandwidth.

3. On the ocean physics governing the enormous variation (30 dB) in ambient noise level.

4. On modeling of intensity fluctuations in the Yellow Sea.

1. INTRODUCTION

This report presents the results of a project to process and analyze acoustic measurements taken by the Applied Physics Laboratory at the University of Washington (APL-UW) during the joint U.S.-China Yellow Sea Experiment.

The Yellow Sea Experiment was a shallow-water acoustics and internal-wave experiment conducted over a 2-week period in August 1996 near the geographic center of the Yellow Sea (37°N, 124°E), in waters approximately 75 m deep. The Institute of Acoustics Academica Sinica, Beijing (IAAS), and the U.S. Georgia Institute of Technology (GTech) provided overall coordination for the experimental program. APL-UW designed, deployed, and operated the two U.S.-fielded vertical acoustic receiving arrays used in this experiment. Additional detail on these arrays and on the field efforts carried out by the APL-UW team is available in Refs. [1] and [2].

This report documents two lines of inquiry. One is the analysis of broadband (80–800 Hz) acoustic propagation measurements for which TNT explosive charges were used as sources. The primary goals here were to extract calibrated transmission loss estimates from the measurements and to infer a geoacoustic model for the seabed representative of the Yellow Sea. Such a model is needed to run numerical codes for shallow-water acoustic propagation and reverberation predictions. The other is the analysis of narrowband (290-Hz) tonal data recorded over a 12-hour period, with the goal of understanding the level and source of acoustic fluctuations in the Yellow Sea. Both inquires have shed light on the properties of low-frequency acoustic propagation in the Yellow Sea.

The report is organized as follows. Section 2 presents a brief review of transmission loss measurements made in the Yellow Sea and documented in the open literature. Section 3 summarizes our method for estimating transmission loss and presents the final results. Included here are remarks regarding the modeling of the source level and waveform associated with explosive TNT sources. Section 4 summarizes our interpretation of the recorded waveforms and transmission loss estimates, from which we deduced a geoacoustic model for the seabed that is consistent with the data. Section 5 discusses the fluctuation measurements. Section 6 is a summary, which also includes a list of topics for which further inquiry will pay off.

2. REVIEW OF TRANSMISSION LOSS MEASUREMENTS IN THE YELLOW SEA

In an experiment similar to the one discussed here, Zhou [3] first deduced compressional wave speeds and attenuation in the frequency range 80–800 Hz for two sites in the Yellow Sea (depths 36.5 m and 28.5 m, but otherwise the exact locations are not specified). Zhou assumed a halfspace model for the seabed characterized by a compressional sound speed c_s, density ρ_s and frequency-dependent attenuation α_s. The bottom topography at both sites was flat, and core samples suggested a bottom composition of fine sand and silt, with $\rho_s = 1.85$ g/cm^3. On the basis of a dispersion analysis of the arrivals from explosive signals, Zhou deduced the ratio $c_s/c_w = 1.056$ for both sites, where c_w is the water sound speed at the water/seabed interface, with c_s being approximately 1584 m/s and α_s being approximately $0.37f^{1.84}$ dB/m (where f is the frequency in kilohertz).

These same measurements were revisited by Zhou et al. [4], with conclusions on c_s/c_w and α_s remaining essentially unchanged. However, the significance of the nonlinear frequency dependence in the sediment attenuation rate ($\alpha_s \sim f^{1.8}$) was discussed as a mechanism for obscuring any optimum frequency for acoustic propagation exhibited in their measurements. Finally, Zhou et al. [5] extended the inverse techniques of Refs. 3 and 4 and arrived at a more complicated model for the seabed consisting of a 10-m-thick sediment layer over a bottom halfspace with a sound speed c_b; within the layer, the sound speed increases from approximately 1555 m/s to 1610 m/s.

More recently, results by various participants in the 1996 Yellow Sea Experiment have been discussed at the Shallow Water Acoustics Conference in Beijing (April 1997) and at the ICA/ASA Conference in Seattle (June 1998). The two primary seabed inversion works by researchers from IAAS presented at the Beijing conference appear to be that of Zhou et al. [6], for which inversion is based on a simulated annealing procedure, and that of Guo et al. [7], for which inversion is based on the model group time delays. Both works suggest a sediment layer with a thickness ranging from 7.5 m [6] to 20 m [7] which separates the water layer from a higher-sound-speed basement halfspace. The parameters describing these geoacoustic seabed models, along with those of Ref. 5, are summarized in Table I.

A picture of the Yellow Sea geoacoustic seabed model thus emerging from Refs. 5–7 is that of a single sediment layer of order 10 m separating a basement halfspace. Interestingly, a more recent work presented in Seattle by Li and Zhang [8], also from the IAAS research team, suggests that a homogeneous halfspace model for the seabed with a sound speed of 1593 m/s is sufficient to obtain a good match between calculated and measured experimental waveforms. We note that this halfspace model

Table I. Geoacoustic models and their references. The sediment layer is of thickness H, with top and bottom layer sound speeds of c_{s1} and c_{s2}, respectively. Basement halfspace sound speed is c_b. Sediment layer attenuation (α_s) and basement halfspace attenuation (α_b) are expressed in dB/λ, with the exception of model A, where α_s is in dB/m and f is in kHz. NA denotes not applicable, and NG denotes not given.

Model	H (m)	c_{s1} (m/s)	c_{s2} (m/s)	α_s	c_b (m/s)	α_b
A, Ref. 5	10	1555	1610	0.34 $f^{1.84}$	1610	NG
B, Ref. 6	7.5	1583	1687	0.23	2131	0.556
C, Ref. 7	21	1560	1601	0.46	1842	1.05
D, Ref. 8	halfspace	1593	NA	1.09	NA	NA

is somewhat consistent with the model presented by our group in Beijing [2] (although the sediment attenuation rate reported by Li and Zhang is significantly higher). It is quite plausible that certain attributes of the measured acoustic data are well explained by a more parsimonious halfspace model for the seabed. However, looking ahead to the results of this work, we also arrive at a layered sediment model for the seabed, but we derive our model in a quite different manner, and our estimate for the sediment thickness (~ 2 m) is substantially less than that proposed in Refs. 5–7.

3. TRANSMISSION LOSS MEASUREMENTS

3.1 Overview of Measurements

Our measurements were made with APL-UW's 16-element vertical line array (VLA), which had an element spacing of 4 m. Each element on the array was approximately omnidirectional. The VLA was deployed from the Chinese research vessel *Shi Yan 3*, which held station at 124°E, 37°N. A second vessel, *Shi Yan 2*, deployed explosive sources (38-g TNT) while under way and holding a steady course (Figure 1). The explosives were preset to detonate at depths of 7 and 50 m, from ranges between 1 and 40 km, with only the 50-m source being used for ranges beyond approximately 15 km. The depth at the *Shi Yan 3*'s position was 75 m with bathymetric changes of O(1) m over the course of the acoustic range.

The acoustic data were first bandpass filtered between 75 and 750 Hz and then digitized at a 2-kHz rate. The receive sensitivity for each hydrophone was a constant –196 dB re V/μPa across the nominal pass band, and a 40-dB gain was applied on each of the 16 recording channels. We recorded 113 sets of arrivals from explosive
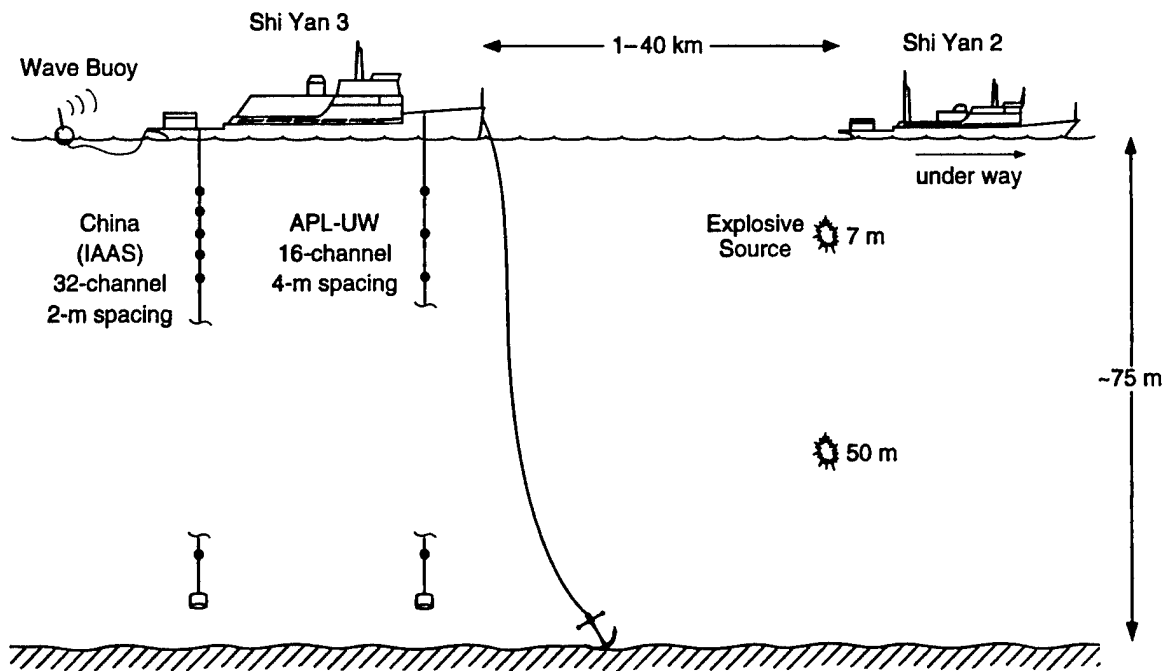

Figure 1. Experimental configuration for the Yellow Sea sound propagation study. Note that 7 m and 50 m correspond only to the preset detonation depths and not to the measured detonation depths. Exact depths for the elements of the APL-UW array are given in figures showing data.

sources (or "shots"). The first 50 shots (first phase) were completed within a time span of approximately 1 hour (2000–2100 local time, 22 August 1996), during which the source vessel steadily opened in range from about 1 to 9 km along a track heading south from the stationary receiving vessel. The next 63 shots (second phase) were completed over a 12-hour period (1130–2330 local time, 23 August 1996), during which the source vessel's range varied from about 2 to 37 km while the vessel transected along a line due east of the source vessel (both opening and closing in range).

Arrivals originating from all 113 shots were subsequently catalogued into 500-ms segments for all 16 channels, for which the first 50 ms and (approximately) the last 200 ms are ambient noise. For each shot, GPS data for the source and receiver vessel were noted, from which the precise range for a given shot was computed. Figure 2 shows three such segments representing the arrivals from shots detonated at increasing range and recorded by channel 2 of the array, which corresponds to a receive depth of 62 m. Time spreading and frequency dispersion, both of which increase with range, are evident, and the total energy in each time series also decreases by about 3 dB per doubling of range, as would be expected from cylindrical spreading.
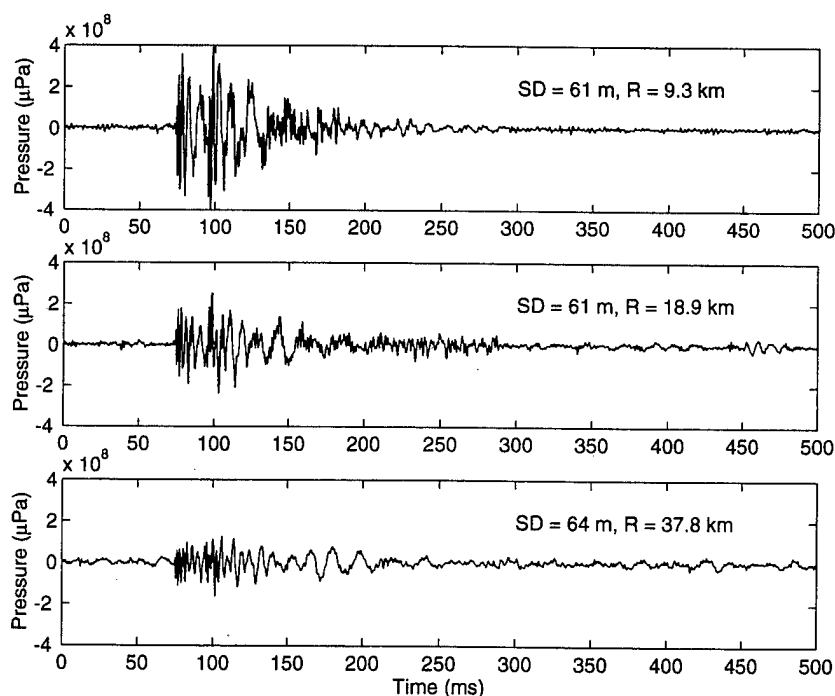

Figure 2. Measured waveforms from sources detonated at increasing range. The receiver depth in each case was 46 m. SD is source depth and R is range.

Note that the summertime sound speed profile exhibits a major influence on acoustic propagation in the Yellow Sea. This profile consists of a warm, high-sound-speed layer ($c \approx 1536$ m/s) on top of a cooler, lower-speed layer ($c \approx 1480$ m/s). Between them is a thermocline which produces a nearly linear decrease in sound speed at a rate $g \approx 3.5$ s^{-1}. Figure 3 shows six temperature, salinity, and sound speed profiles taken 1 hour apart from aboard the *Shi Yan 3* by researchers from the South China Sea Institute of Oceanology. The vertical movement of the thermocline is associated with the internal tide. This figure also shows our geoacoustic model for the seabed of the Yellow Sea; we postpone further remarks on its derivation until Section 4.
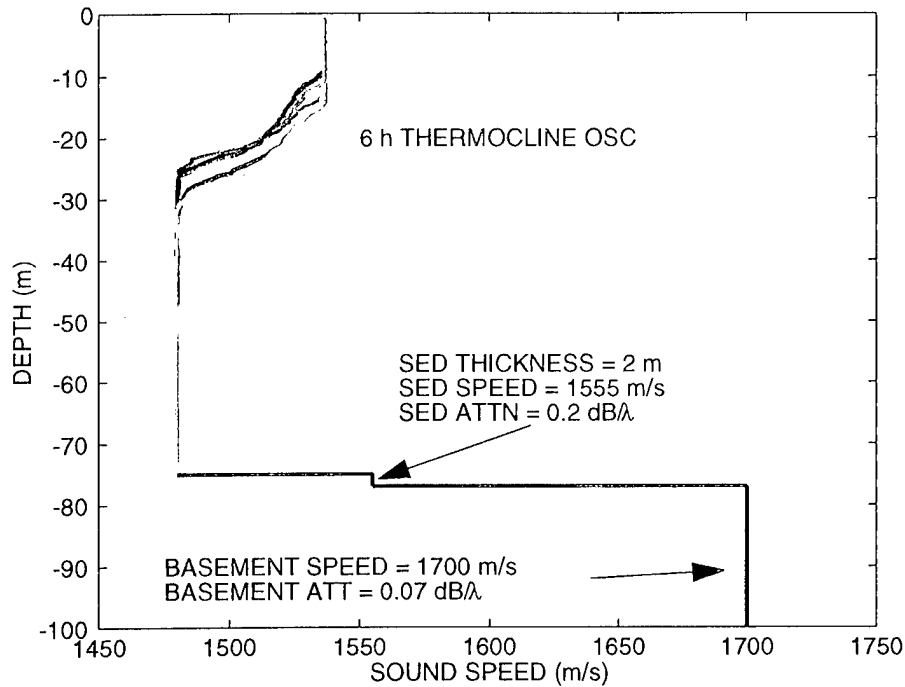

Figure 3. Measured sound speed profiles over a 6-hour period (each color separated by 1 hour) which show vertical oscillations in the thermocline. The sound-speed profile at depths below approximately 30 m is nearly isovelocity with a speed of 1480 m/s. Our geoacoustic model for the seabed begins at the water/sediment interface at a depth of 75 m.

3.2 Method for Estimating Transmission Loss from Explosive Sources

In this section we outline our method for estimating transmission loss (TL) using broadband explosive sources, which is based on third-octave band processing of the recorded data. Calibrated estimates of TL are vulnerable to systematic error, and the following documentation represents our efforts to reduce such errors. The method below pertains to a single channel and is applied in the same manner to all 16 channels of the VLA. After the recorded voltage is converted to pressure $p(t)$ in dynes/cm^2 based on the hydrophone receive sensitivity and 40-dB gain, the following is carried out:

1. Each 500-ms segment of $p(t)$ is filtered by a third-octave band IIR filter. The center frequencies and bandwidths are given in Table II. The filtered output for the ith filter band is $p_i(t)$.

2. A corresponding 500-ms time series of noise, $p_N(t)$, is synthesized using a combination of the 50-ms noise precursor and the approximately 100 ms of noise recorded after the signal arrival. This time series is then filtered in the same manner as $p(t)$ to give an estimate of filtered noise, $p_{Ni}(t)$, within the ith filter band.

Table II. Center frequencies and bandwidths for third-octave filter.

	Center Frequency (Hz)	Bandwidth (Hz)
1	80	19
2	100	23
3	125	29
4	160	37
5	200	46
6	250	58
7	320	74
8	400	93
9	500	116
10	630	146
11	800	185

3. The total energy density of the signal arrival within the ith filter band, e_i (in ergs/cm^2), is computed as

$$e_i = \frac{1}{\rho c} \int_0^T [p_i^2(t) - p_{Ni}^2(t)]dt, \tag{1}$$

where the integration time window T is 500 ms. Note that water density ρ and sound speed c are in cgs units with $\rho = 1$ g/cm^3 and $c = 150,000$ cm/s; the latter is an approximate average over the water depth.

4. The total energy density per Hz in the ith filter band is e_i/b_i, where b_i is the third-octave filter bandwidth (Table II). The decibel equivalent of this quantity is $E_i = 10 \log e_i/b_i$.

5. Transmission loss in the ith filter band is computed as $TL_i = SL_i - E_i$, where SL_i is the decibel equivalent of the explosive charge source level in dB re ergs/cm^2/Hz at a reference distance of 1 m (estimation of SL_i is discussed below). Final estimates of TL are in dB re 1 m.

3.3 Modeling the Source Level From Explosive Charges

To compute the SL_i we first compute a model time series for the source pulse $p_0(t)$ at 1-m range from the explosive charge. Empirical equations, the majority of which were derived by Chapman [9], are incorporated in this program, which reproduces well examples of experimentally measured source pulses given by Chapman and also by Wakeley [10]. These equations include the well-known relation between the period of the first bubble pulse T_1, the charge weight w, and the charge detonation depth D (all units in mks)

$$T_1 = 2.11w^{1/3}(D + 10.1)^{-5/6}, \tag{2}$$

which we use to confirm the actual charge detonation depth.

We estimated T_1 for each shot arrival by estimating the time lag to the first primary peak of the signal's autocorrelation function. In doing so for all 113 of our recorded shot-arrival data, we discovered that the preset source depths, given to us as 7 and 50 m, varied significantly from our measured detonation depths as calculated from Eq. (2). Figure 4 shows a histogram of the measured detonation depths. The shallow-source detonations (N=44) are consistent with a nominal 7-m preset depth, with a mean equal to 7.4 m. However, the deeper source detonations (N=69) differ by about 10 m from the 50-m preset depth. In some cases the measured depths are deeper than the water depth itself, and we assume these represent incomplete
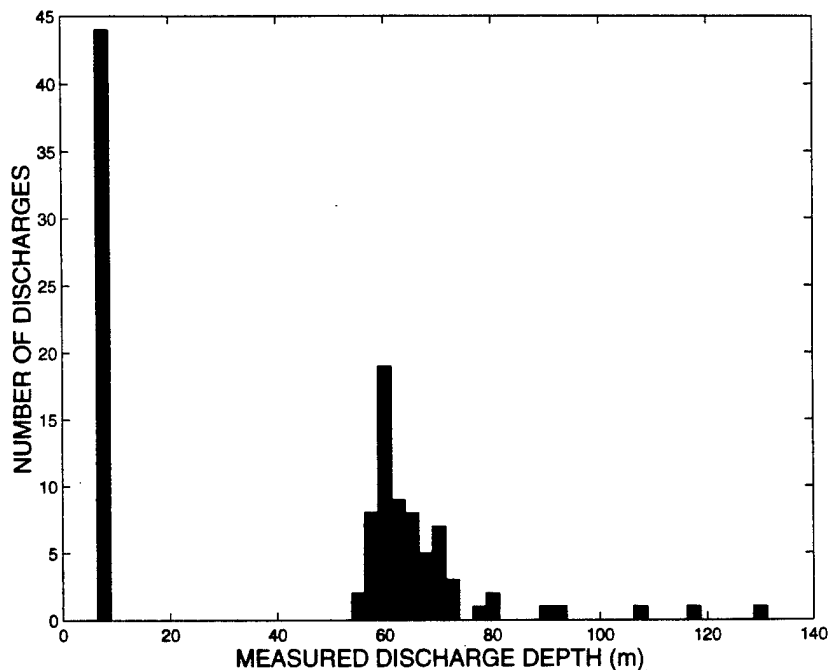
Figure 4. Histogram of the measured detonation depth for all 113 shots (bin width is 2.5 m). The 7-m preset detonations are shown clustered on the left about an average depth of 7.4 m. The 50-m preset detonations are shown on the right and have a greater spread. Detonations at depths greater than 68 m are assumed to have been incomplete.

discharges. Inspection of the histogram of measured detonation depths suggests that depths greater than about 68 m most likely fit into this category. We have thus removed from our total database for estimating transmission loss those arrivals for which the estimated discharge depth exceeded 68 m (19 of 69).

Figures 5 and 6 show the model waveform and resulting energy spectrum (up to 1000 Hz) for a 38-g TNT charge detonated at 7 m (Figure 5) and 61 m (Figure 6). The 11 symbols, plotted over each energy spectrum, are the values for SL_i used in our transmission loss calculations, which are computed by averaging the energy spectrum over the bandwidths and about the center frequencies listed in Table II. To improve the accuracy of our transmission loss estimates, we made separate computations of the source level for each shot number, running the source level model at a depth corresponding to the particular shot arrival's estimated source detonation depth. Note that the 10-m difference in preset vs measured detonation depth results in about a 3-dB difference in source level for frequencies less than about 300 Hz.

Figure 5. Model waveform (top) and energy spectrum (bottom) for a 38-g TNT charge detonated at 7 m. The 11 symbols plotted over the energy spectrum are the actual values for the source level used in the transmission loss calculations.
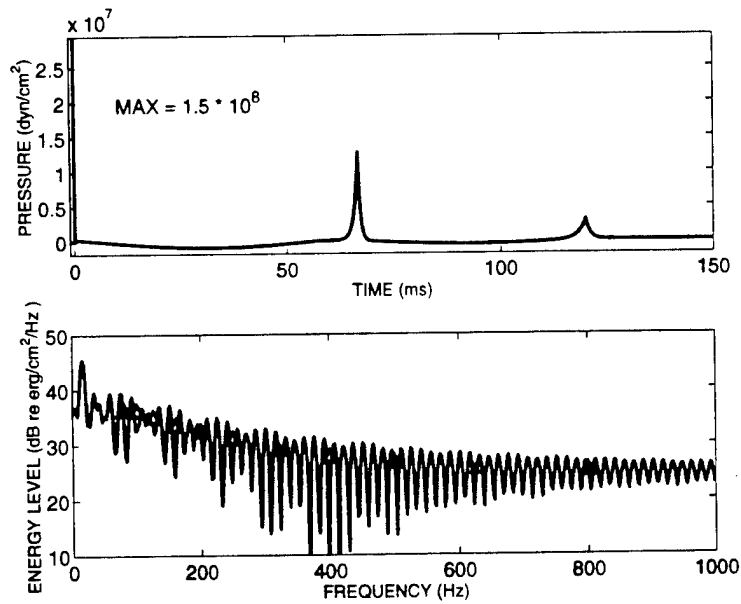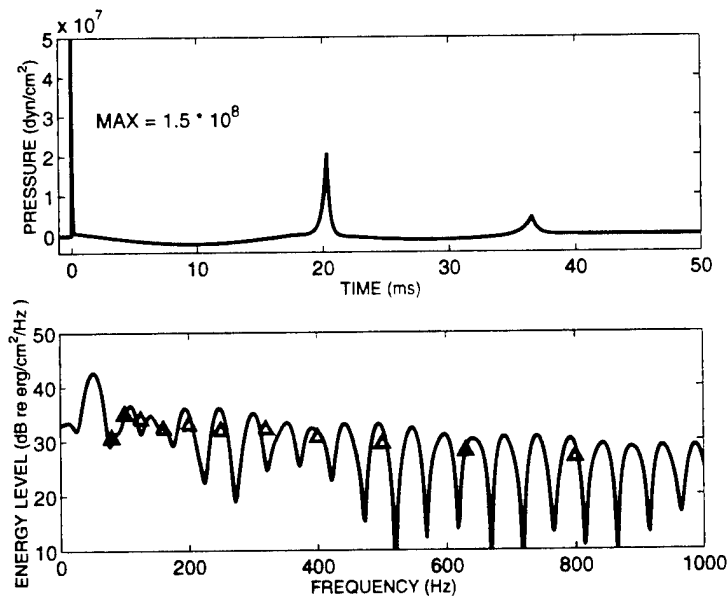

Figure 6. Model waveform (top) and energy spectrum (bottom) for a 38-g TNT charge detonated at 61 m. The 11 symbols plotted over the energy spectrum are the actual values for the source level used in the transmission loss calculations.

3.4 Results

Figure 7 is a plot of estimated TL vs range for third-octave bands with center frequencies of 200 Hz, 400 Hz, and 800 Hz. The receiver depth is 46 m (VLA channel 6). The estimated source detonation depths range between 55 m and 68 m and are color coded: green for 55–60 m, blue for 61–64 m, and red for 64–68 m. There appears to be no significant source-depth dependence in our TL estimates (for source depths between 55 m and 68 m), once we have accounted for the exact source depth in our model for source level (SL_i). We shall thus use the average source depth, 61 m, in the model TL computations. The solid curve in each plot is the result of our geoacoustic model implemented in the SNAP [11] numerical propagation computer program, assuming a source depth of 61 m. The triangles represent TL estimates made along the first-phase southerly transect, and the circles represent TL estimates made along the second-phase easterly transect. Unfortunately, a temporary failure in our electronics during the first phase cut short this measurement series; nevertheless the combined data are consistent and show little if any azimuthal dependence in acoustic propagation within this region of the Yellow Sea. The fact that estimated TL values fall consistently above the model curve for ranges less than about 5 km may be in part due to some saturation in our recording system, which was limited to shots detonated at close range.

Figure 7 also shows examples of multiple-shot detonations at the same range. The estimated TL in these cases varies about ±1.5 dB, which we impart to natural variability in the process we are attempting to measure. The uncertainty in hydrophone receive sensitivity is at least ±1 dB, and the uncertainty in modeling source level, given we know exactly the source's detonation depth and charge weight, is also about ±1 dB [9]. Combining these uncertainties gives an overall error of about ±2 dB for our transmission loss estimates.

Figure 8 shows TL versus frequency for three ranges. The receiver depth is again 46 m, but all source depths within the range 55 to 68 m are denoted by the same symbol. The solid curves represent our geoacoustic model implemented by SNAP, which tend to track the general trends in the frequency and range dependence exhibited by the data. The exception is for frequencies less than 200 Hz. We are less confident in our TL estimates for these frequencies owing to the attendant greater difficulty in modeling the precise source level.

Figures 9 and 10 show the range and frequency dependence in the estimated TL (top plot) and modeled TL (bottom plot) at two receiving depths, while Figures 11 and 12 show range and depth dependence at two frequencies in the same manner. On one hand, Figures 11 (top) and 12 (top) suggest a possible mode interference pattern that is not reproduced by the SNAP computations which employ our geoacoustic model of Figure 3. On the other hand, the pattern amplitude in each case is not so large that it can't be attributed to variations in receive sensitivity along the VLA. We will want to investigate this further, however, in future work.
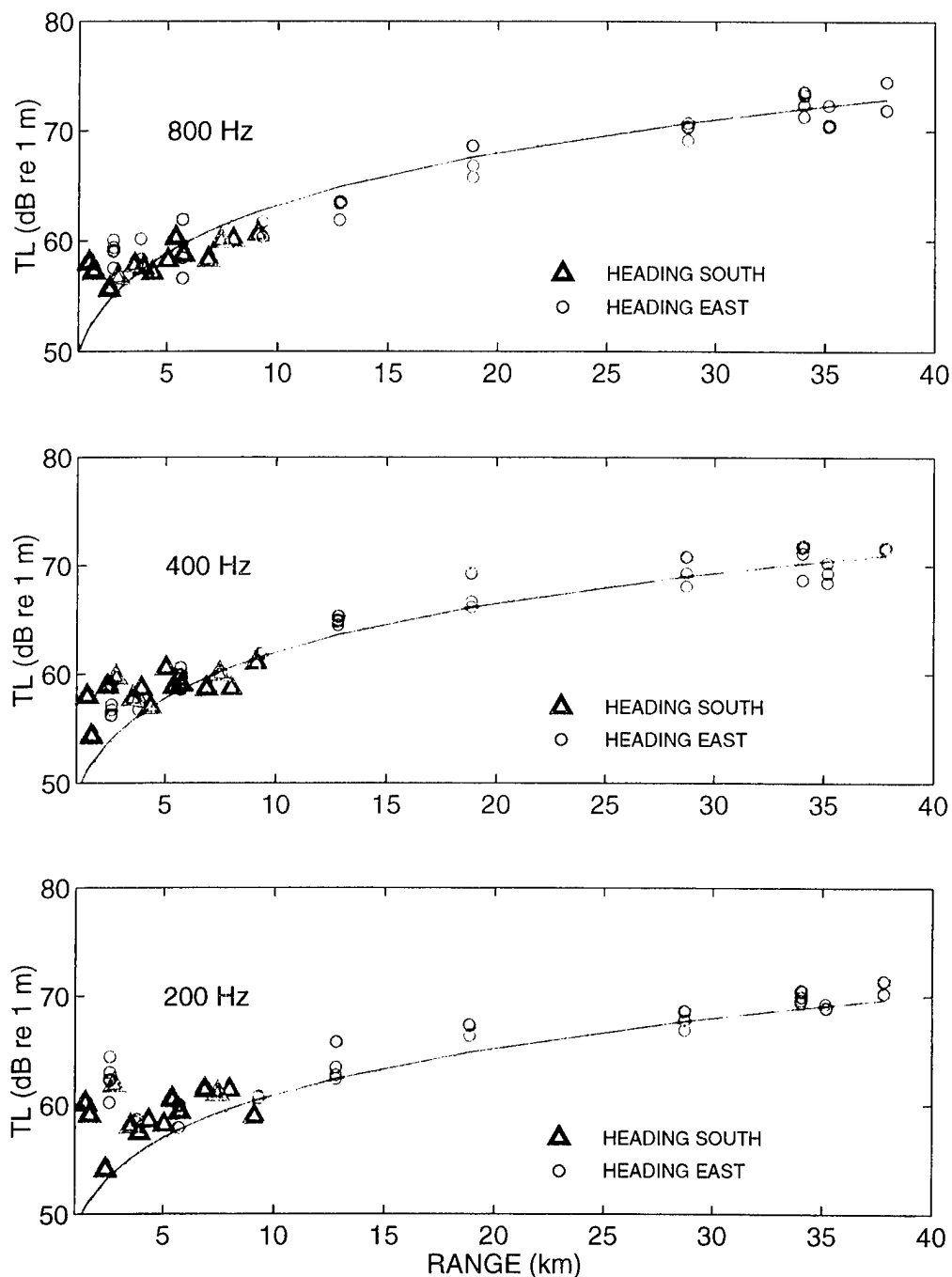
Figure 7. Estimated transmission loss vs range for three third-octave bands. The receiver depth is 46 m and the source depths are color coded: green for 55–60 m, blue for 61–64 m, and red for 64–68 m. The curves are the results of the geoacoustic model in Figure 3 as implemented by the SNAP acoustic propagation model.
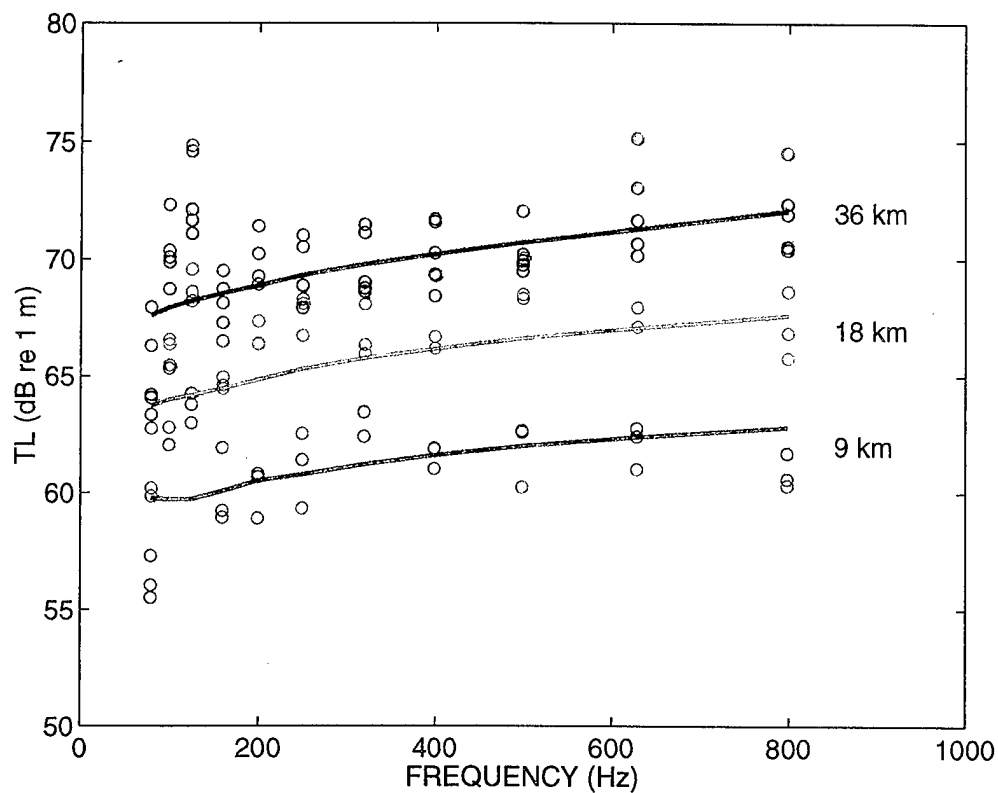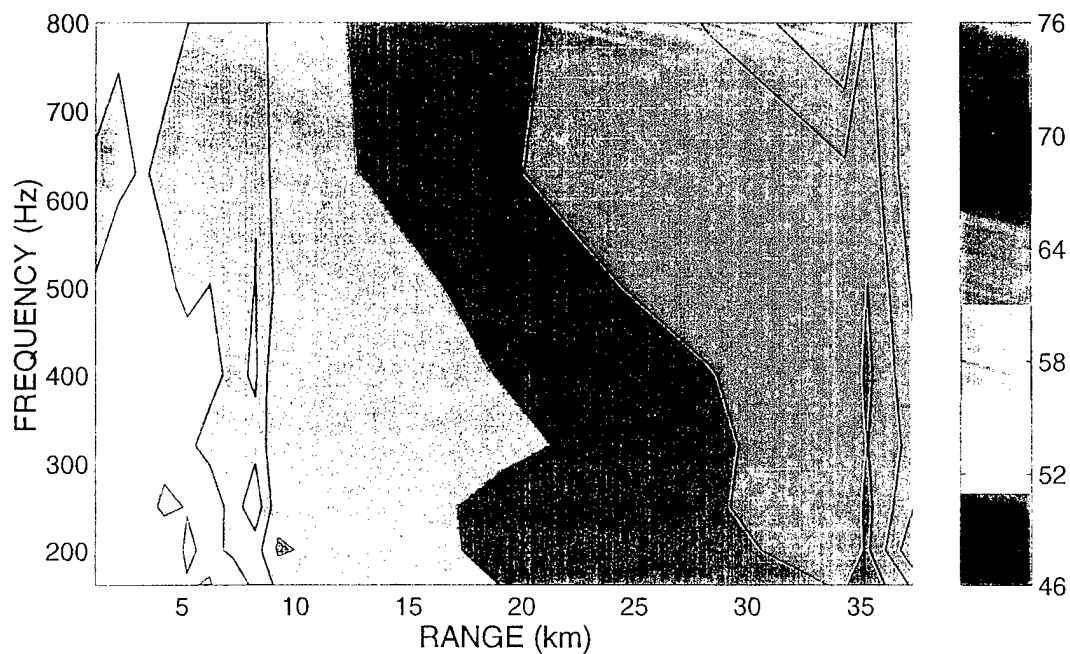
Figure 8. Estimated transmission loss vs frequency for three ranges. The receiver depth is 46 m, and all source depths between 55 and 68 m are denoted by the same symbol. Color is used only to distinguish data taken at different ranges. The curves are the result of the geoacoustic model in Figure 3 as implemented by the SNAP acoustic propagation model.

TL DATA (dB re 1 m)

TL SNAP MODEL (dB re 1 m)

Figure 9. Contours of estimated (top) and modeled (bottom) transmission loss vs frequency and range for a source depth of 61 m and a receiver depth of 30 m. Model contours are the results of the geoacoustic model in Figure 3 as implemented by the SNAP acoustic propagation model. Contour intervals are shown on right in dB re 1 m.

Figure 10. Contours of estimated (top) and modeled (bottom) transmission loss vs frequency and range for a source depth of 61 m and a receiver depth of 56 m. Model contours are the results of the geoacoustic model in Figure 3 as implemented by the SNAP acoustic propagation model. Contour intervals are shown on right in dB re 1 m.
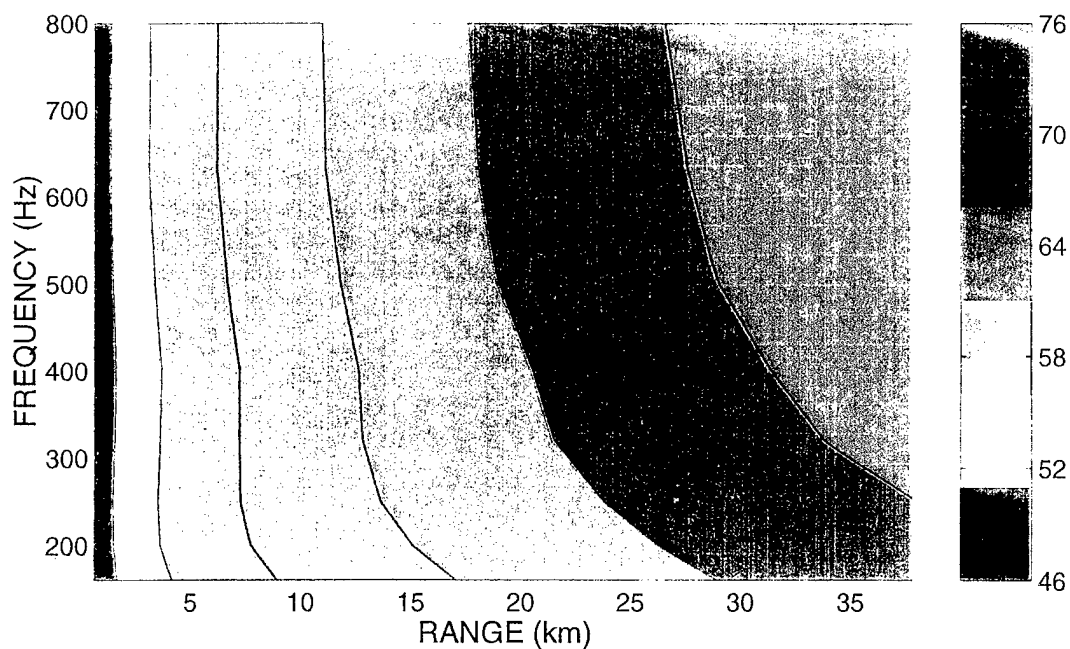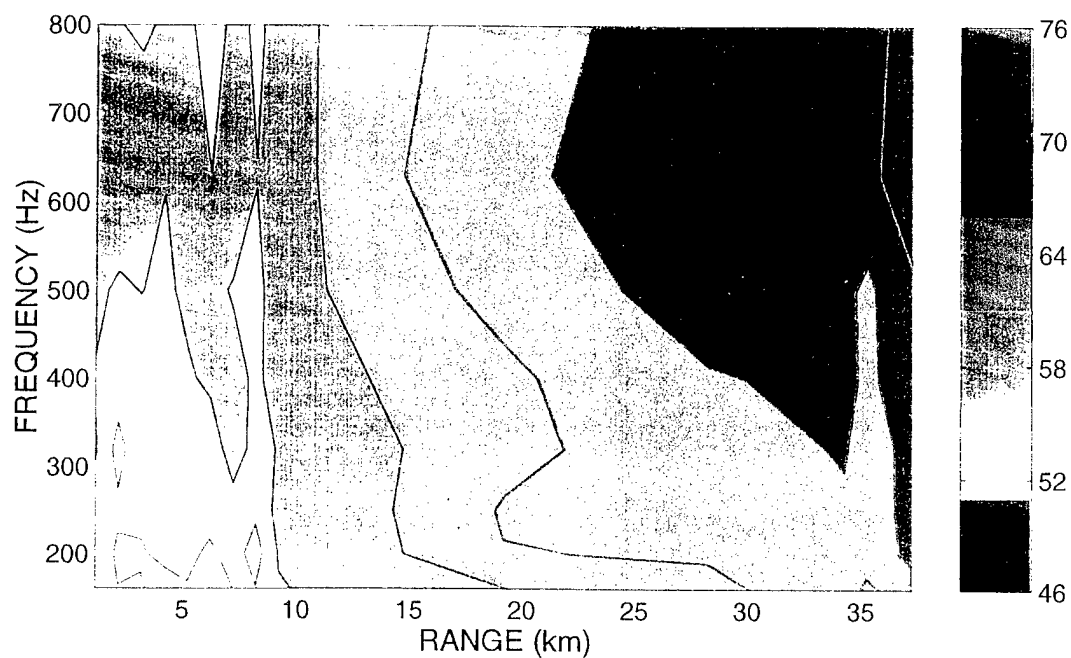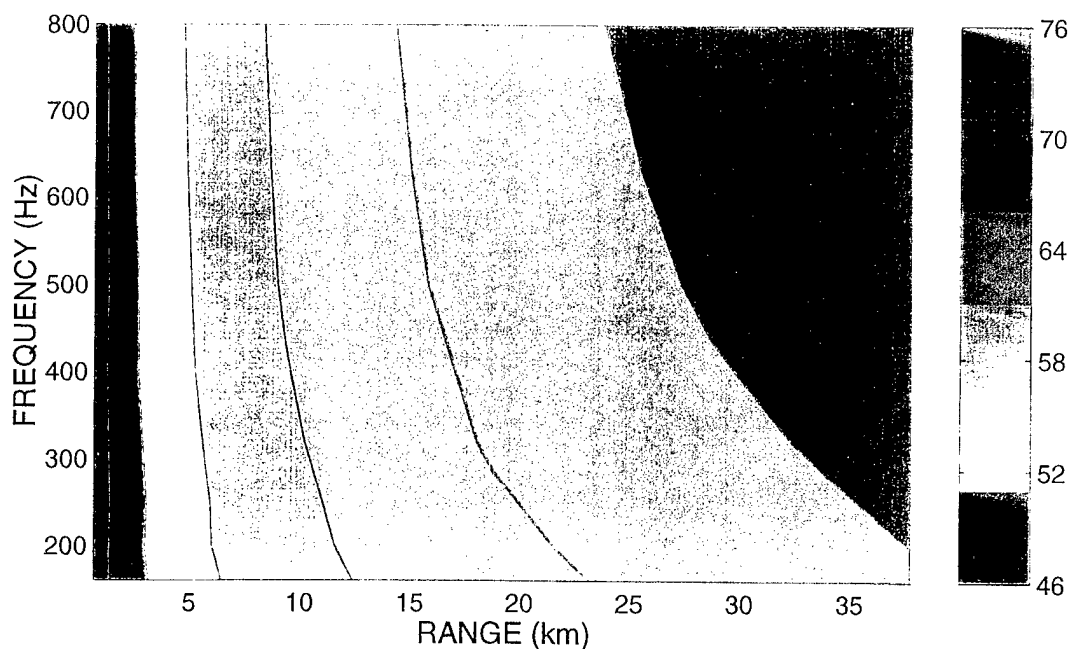
TL DATA (dB re 1 m)

TL SNAP MODEL (dB re 1 m)
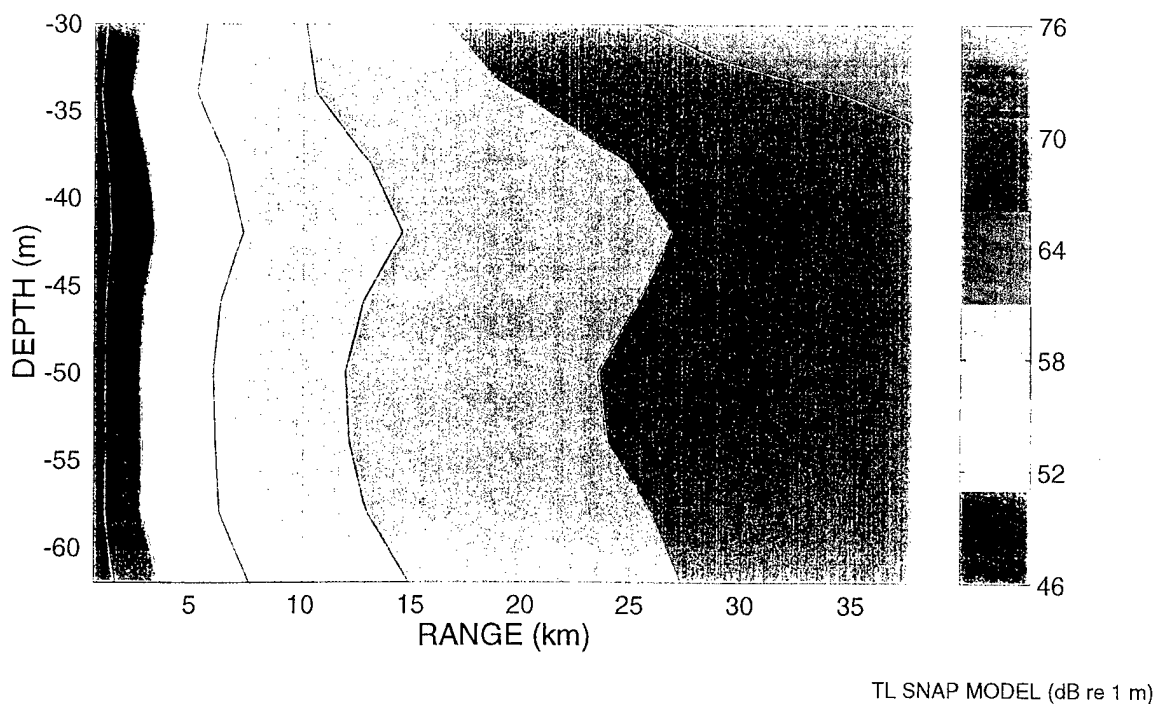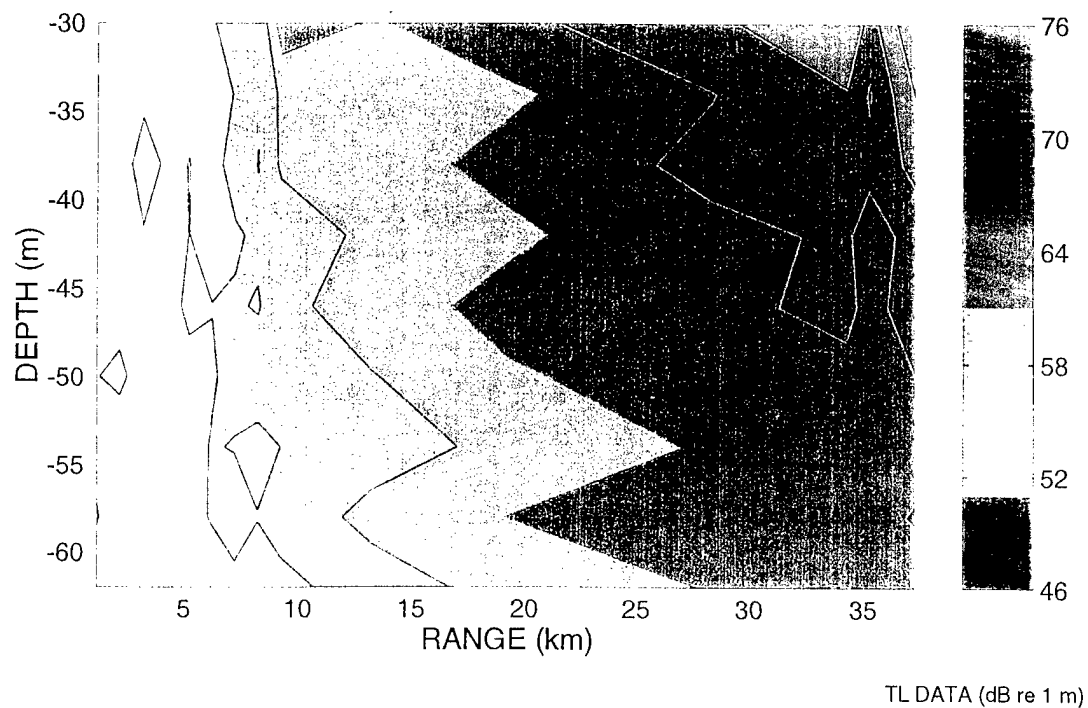
Figure 11. Contours of estimated (top) and modeled (bottom) transmission loss vs depth and range for a source depth of 61 m and a frequency of 400 Hz. Model contours are the results of the geoacoustic model in Figure 3 as implemented by the SNAP acoustic propagation model. Contour intervals are shown on right in dB re 1 m.

Figure 12. Contours of estimated (top) and modeled (bottom) transmission loss vs depth and range for a source depth of 61 m and a frequency of 800 Hz. Model contours are result of the geoacoustic model in Figure 3 as implemented by the SNAP acoustic propagation model. Contour intervals are shown on right in dB re 1 m.
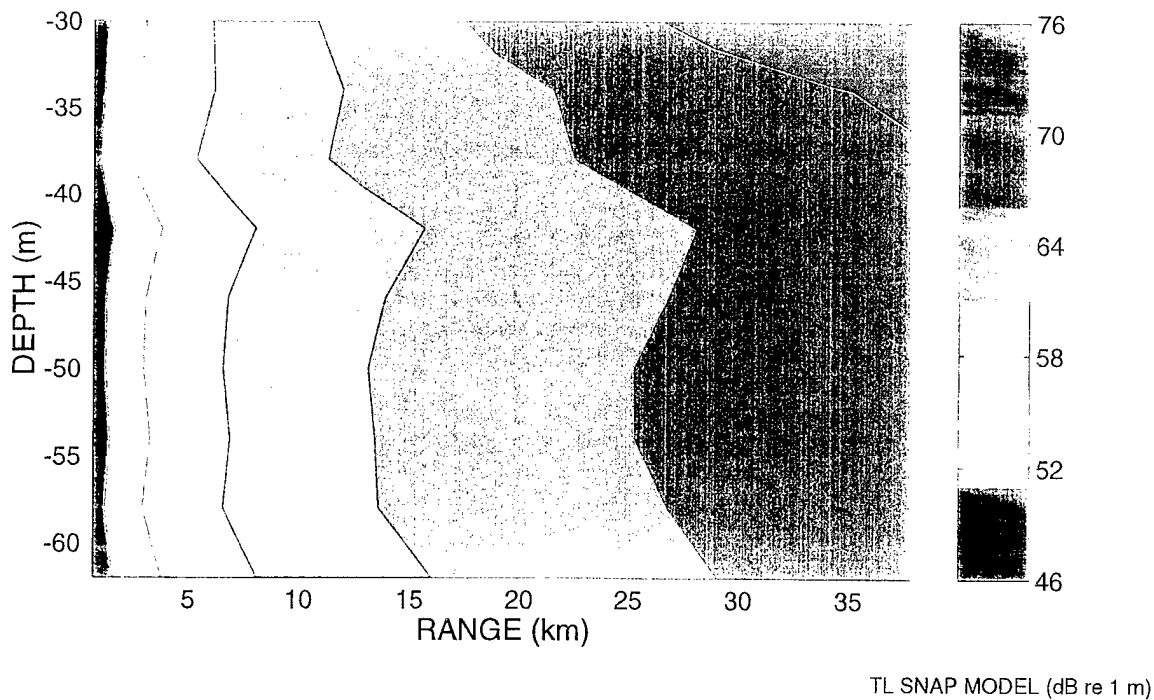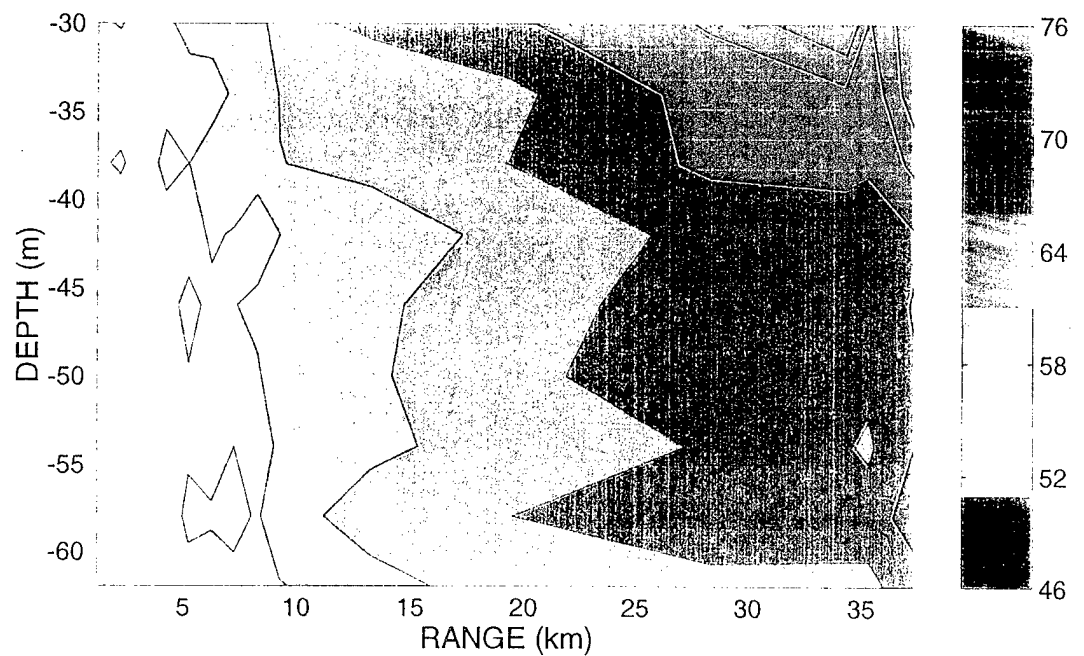
4. DATA INTERPRETATION AND GEOACOUSTIC SEABED MODEL

In this section we interpret both the waveform data and the TL estimates in order to deduce a geoacoustic model for the seabed. We use a combination of methods as discussed below.

4.1 Headwave Arrivals

The first method involves analysis of headwave arrival times. Figure 13 shows schematically the two rays associated with a headwave received by two vertically separated hydrophones, where there is a common path taken along the water/sediment interface. (We shall refer to the headwave as a single entity, which manifests itself differently for each receiver on the VLA.) Shown also (for the lower hydrophone only) are the first four, primarily water-borne, ray paths, which are the direct, refracted, surface-reflected, and bottom-reflected paths. For a particular combination of range and source depth, the first arrivals seen in the waveform data are those associated with a headwave. Figure 13 depicts, for simplicity, a headwave propagating along the water/sediment interface with the sediment represented by a halfspace. If a sediment
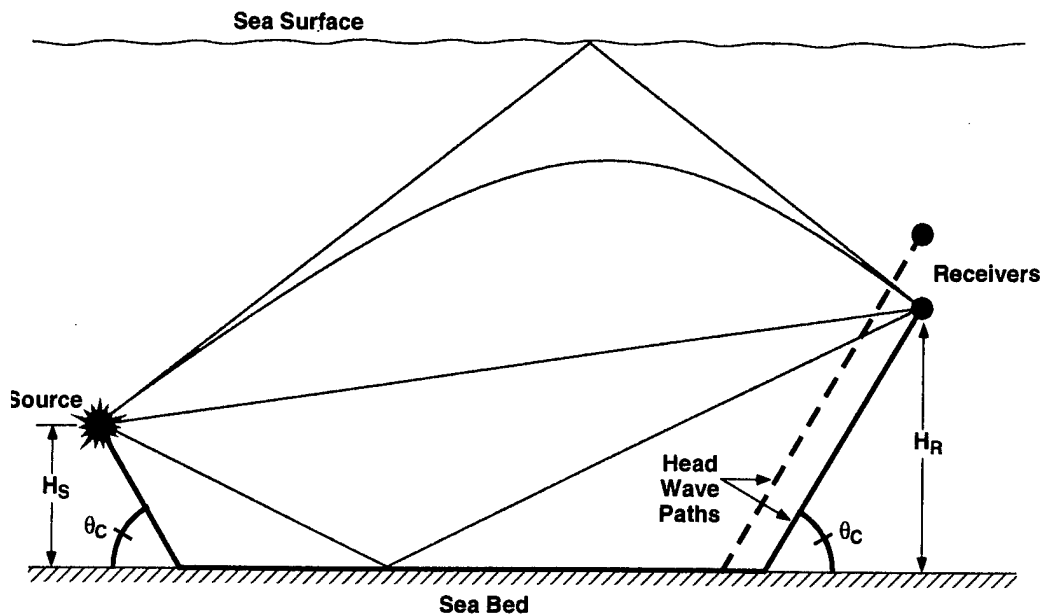

Figure 13. Schematic view of two ray paths associated with the headwave received by two vertically separated hydrophones. The two rays share a common path along the water/sediment interface. Also shown (for the lower hydrophone only) are the first four, primarily water-borne, paths.

layer exists between the water and halfspace, then the classical headwave [12] will instead propagate along the sediment layer/halfspace interface. (There can exist conditions for which this does not occur, which we will not discuss here. Furthermore, if there exists a strong enough sound speed gradient within the sediment layer, a refracted arrival can occur which mimics somewhat the behavior a headwave.) A simple model for the headwave travel time τ is

$$\tau = \frac{R}{c_b} + \frac{(H_S + H_R)c_w}{\sqrt{1 - (\frac{c_w}{c_b})^2}} \left(\frac{1}{c_w^2} - \frac{1}{c_b^2} \right) + \frac{2Hc_s}{\sqrt{1 - (c_s/c_b)^2}} \left(\frac{1}{c_s^2} - \frac{1}{c_b^2} \right), \qquad (3)$$

where R is range, H_S and H_R are the source and receiver heights above the bottom, c_w is the sound speed in the water, c_s is the sound speed within the sediment layer of thickness H, and c_b is the sound speed in the basement halfspace (all units are in mks). The sequence of headwave arrivals vs decreasing hydrophone depth forms a line with a slope related to retardation of arrivals for the shallower receiver depths, as the ray associated with the headwave spends less time within the higher-speed halfspace region. This is shown in Figures 14 and 15, which are consistent with a basement sound speed of approximately 1650 m/s.
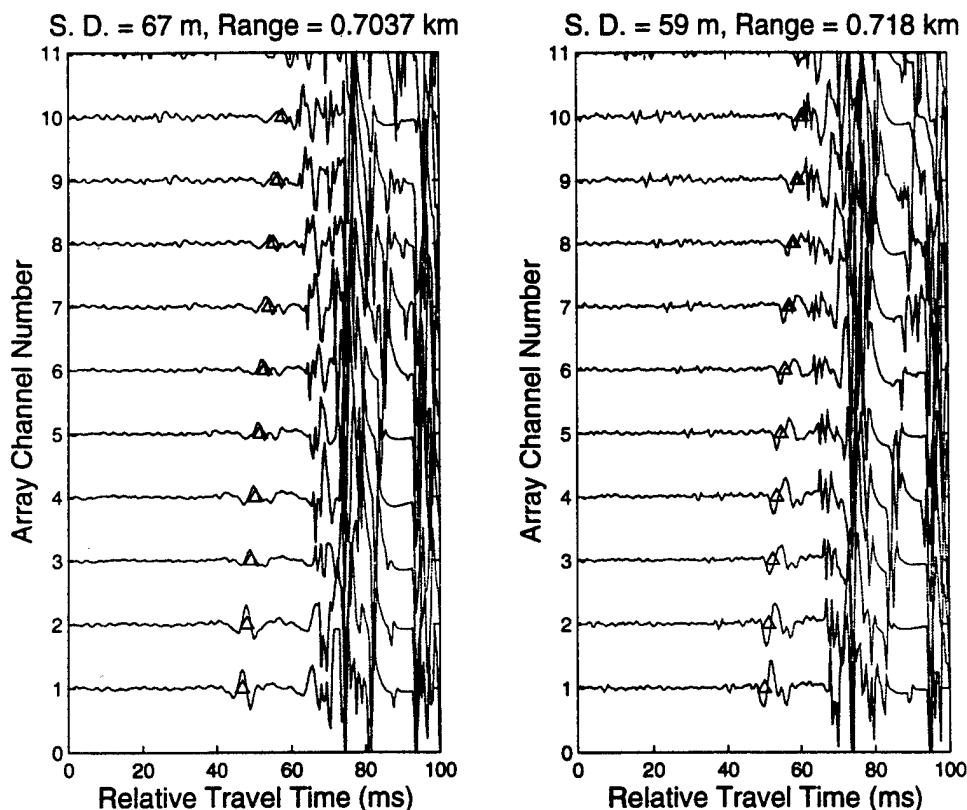
Figure 14. Arrival structure vs depth for two combinations of source depth (SD) and range (R). The triangles mark a particular phase (e.g., zero crossing or positive/negative peak) of the headwave arrival.

S. D. = 63 m, Range = 0.7654 km S. D. = 61.5 m, Range = 0.909 km
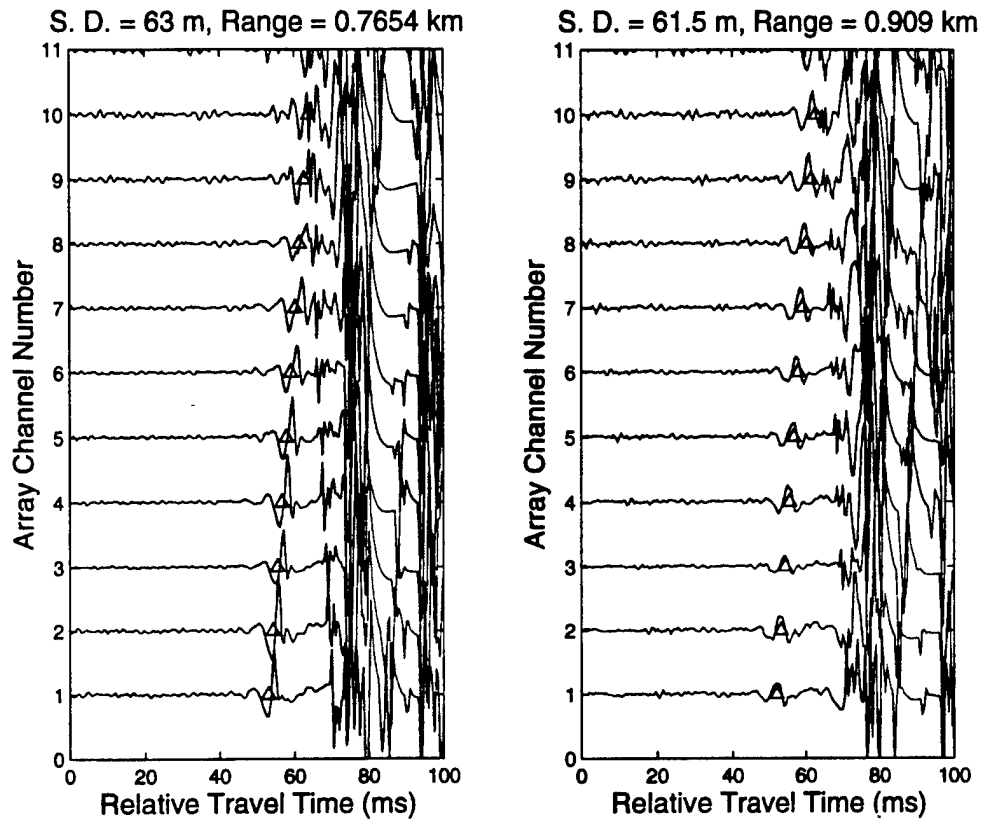
Figure 15. Same as Figure 14.

The ensemble-averaged energy spectrum for a headwave is shown in Figure 16. This is computed by averaging spectra from the headwave arrivals for channels 1–5 for a single shot, and then further averaging across the four shots represented in Figures 14 and 15. The spectral bandwidth is remarkably narrow, with a peak at approximately 130 Hz. There is much more to be understood about the nature of this spectrum, which is left to future work, e.g., how is the seabed affecting the spectral peak and the bandwidth?
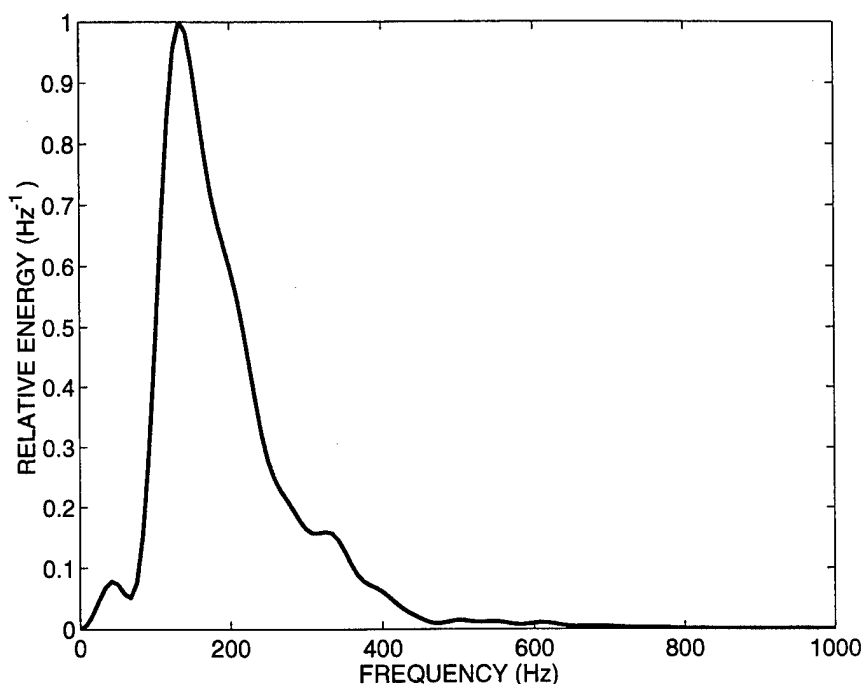
Figure 16. Energy spectrum for the headwave computed by averaging spectra for the headwave arrivals shown in Figures 14 and 15 (channels 1–5 only).

4.2 Synthetic Arrivals Computed Using the KRAKEN Normal-Mode Program

The second method involves generating synthetic arrivals using the KRAKEN normal-mode program [13]. For a given geoacoustic model and water-column sound-speed profile, the KRAKEN program computes a narrowband, or cw, acoustic field for a point source based on the summation of normal modes. (Note that since KRAKEN is based on normal modes, it cannot simulate headwave effects.) For this project a program was developed to coherently sum together the narrowband fields in order to simulate the field from a broadband source. We use the same program discussed in Section 3.3 for the broadband source pulse, which gives the necessary frequency-dependent source amplitudes and phases.

Figure 17 compares measured (top) and synthetic (bottom) arrival structure, or vertical moveout pattern, for which the geoacoustic model in Figure 3 was used in generating the synthetics. The source in this case was detonated at a depth 67 m and a range 0.72 km. The key parameters governing the match between the synthetics and the data are the sediment thickness H and basement sound speed c_b, which we estimate to be approximately 2 m and 1700 m/s, respectively. This estimate was carried out by comparing several measured and synthetic waveforms,
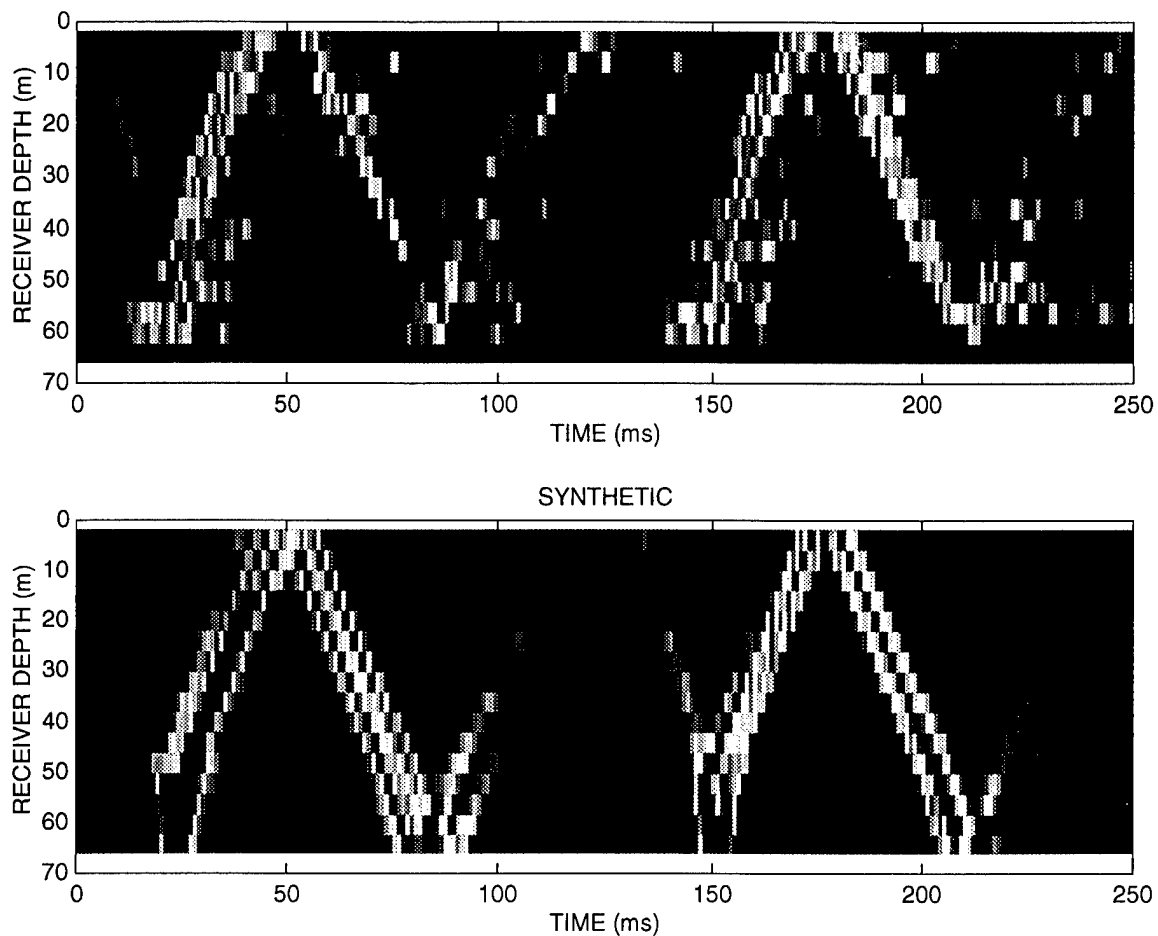
Figure 17. Measured (top) vs synthetic (bottom) vertical arrival structure, or moveout pattern. The source depth is 67 m and the range is 0.72 km.

for which candidate estimates of H and c_b were tried. Sediment (α_s) and basement (α_b) attenuations were also estimated in this manner by examining the measured and synthetic waveforms associated with longer ranges. The synthetic waveforms were weakly sensitive to the sediment layer sound speed c_s, and our provisional estimate of this value is 1555 m/s. We also assign 1700 m/s to c_b, rather than the slightly lower (though consistent) 1650 m/s value inferred from the headwave arrival patterns.

4.3 Transmission Loss Calculations Using the SNAP Normal-Mode Program

The third method involves computing model estimates of transmission loss using the SNAP normal-mode program. For model vs data comparisons, the SNAP program is run at each of the 11 center frequencies given in Table I, and the acoustic field is computed by an *incoherent* summation of the normal modes. This gives a result equivalent to our experimental third-octave band processing [14]. Our primary purpose for using the SNAP program in this manner was to evaluate candidate geoacoustic models for the seabed that were deduced by a combination of the first two methods.

We also used SNAP in conjunction with various model-minus-data error-minimization algorithms in order to deduce a geoacoustic model for the seabed using the TL estimates alone. Depending on the particular algorithm used, this method converged on a set of parameters consistent with our model shown in Figure 3, although there were some notable differences. For example, this approach resulted in a sound speed gradient of $g \approx 1$ s^{-1}. However, since considerable information such as headwave arrivals and the waveform vertical moveout pattern is washed out in the TL estimates, we favor the gradient-free model depicted in Figure 3.

We conclude this section by comparing our geoacoustic model in Figure 3 with two of the models (B and D) described in Table I, which were derived by scientists from IAAS using measurements from this same experiment (though not on the same vertical line array). The comparison is made using the SNAP program, and the results are shown in Figure 18. Our model compares best with the estimated TL data insofar as matching general trends in frequency dependence and overall level, with an overall model-minus-data error of ±2 dB. Of the two IAAS models we compared, model B performs best, with approximately the same error. However, it would be impossible to match properties seen in the waveform data, such as vertical moveout, with the thicker sediment used in model B, and thus we are more confident in our model. Model D clearly differs from the trends exhibited in the data.
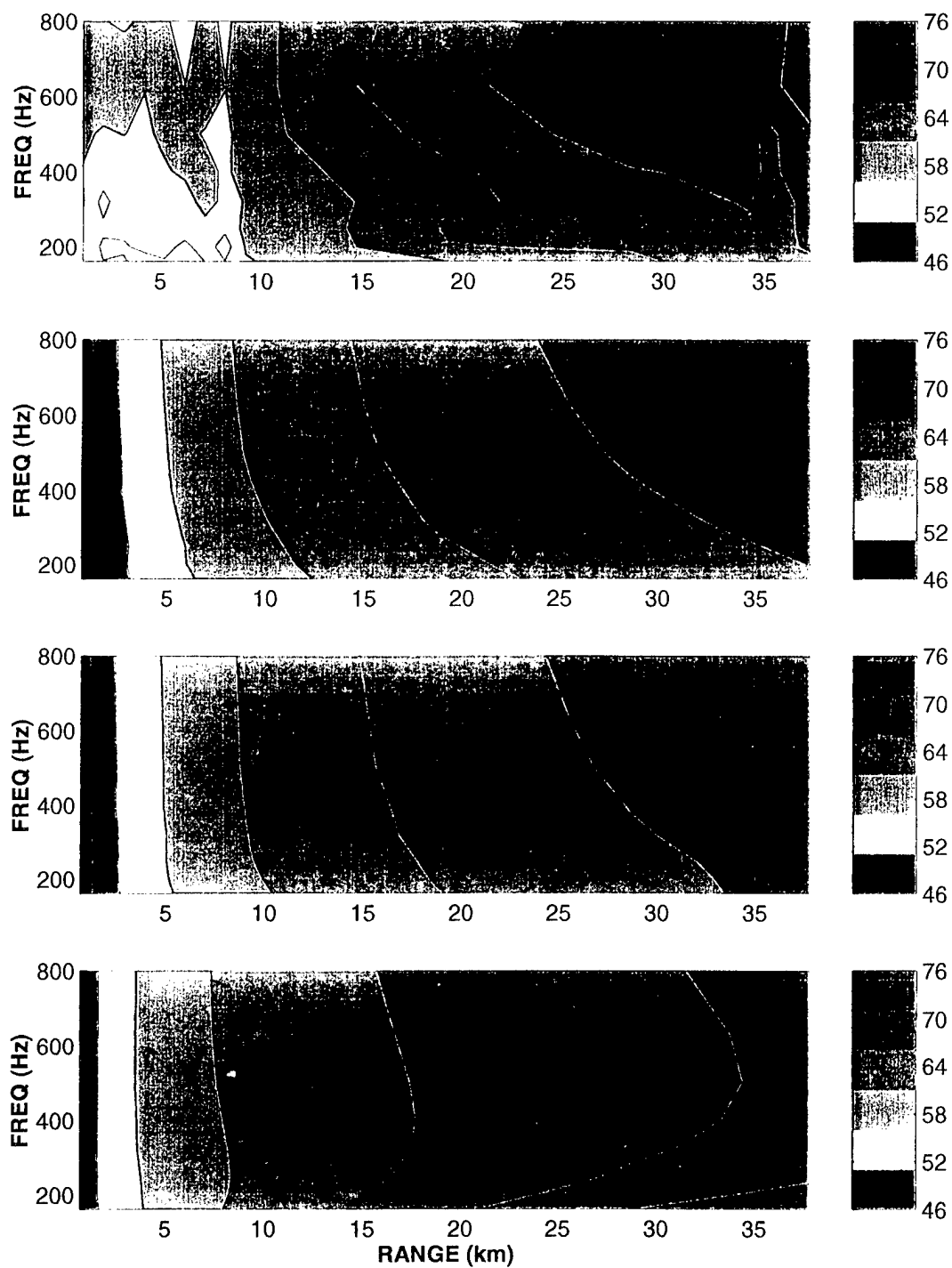
Figure 18. Contours of transmission loss vs range. Top panel is data; second from top panel is SNAP computations using the geoacoustic model in Figure 3; third from top panel is SNAP computations using geoacoustic model B in Table II; bottom panel is SNAP computations using geoacoustic model D in Table II. Contour intervals are shown on right in dB re 1 m.

5. FLUCTUATION MEASUREMENTS

In this section we present some initial results of the cw tonal measurements made with APL-UW's four-element, bottom-moored vertical array (Figure 19). This array was designed to operate autonomously, recording acoustic data at a 2-kHz sampling rate for each of the four hydrophones. Additional technical specifications and remarks concerning this system are given in Ref. 1. The array was deployed 3.8 km east of the *Shi Yan 3*, which held station at 37°N, 124°2.5'E during the course of these measurements. The depth at the deployment site was 76 m. Recording on the four hydrophones began on 29 August at 2200 and continued uninterrupted until the mooring's recovery on 31 August at 1200.

The data-acquisition system linked to two of the hydrophones failed, but data were recovered for the two remaining hydrophones, which were at depths of 38.5 m and 46.7 m (Figure 19). Figures 20 and 21 are spectrograms for the entire time span (approximately 38 hours) recorded by these hydrophones; each is a succinct representation of nearly 274 Mbytes of information. The color coding indicates relative acoustic power spectral density (PSD), ranging from dark blue (lowest PSD) to dark red (highest PSD). Each spectrogram shows a remarkably consistent periodicity in PSD, with a period of approximately 6.2 hours, which is precisely one half the period of the M2, or principal lunar, tidal mode. The PSD over a broad band varies by about 25 to 30 dB over this 6.2-hour period, which is an enormously large change. At first glance one might suspect flow noise: the inbound and outbound current flow associated with the M2 tide produces two high-flow events per M2 period, giving the observed 6.2-hour periodicity. However, flow noise would not be so broadband and likely could not produce the enormous increase observed in the PSD level. Our conjecture is that tidal-mediated oscillations in the sound-speed profile are causing profound changes in the nature of ambient noise propagation in the Yellow Sea. This needs to investigated further, however.

The dark lines located at 290 Hz and spanning a length of 12 hours correspond to the Russian-made acoustic source (owned and operated by IAAS), which was suspended over the side of the moored *Shi Yan 3* at a depth of 50 m. The source was turned on at 0300 on 30 August and transmitted a continuous 290-Hz tone for the next 12 hours. It is not known at this time what source (if any) produced the fainter line located at about 800 Hz in each figure which persists over the entire recording period.

Figure 22 represents a closer view of the 290-Hz tonal data. For this figure, the original data sampled at 2 kHz, with a 1-kHz bandwidth, are passed through a processing sequence wherein the recorded data are demodulated, filtered, and

Sub-Surface Buoy

Tensioned Sub-Surface Line

76 m

38 m

23.2 m — H4

30.7 m — H3

38.5 m — H2

46.7 m — H1

Data Loggers (2)

Glass Floats (6)

Acoustic Releases (2)

17.6 m
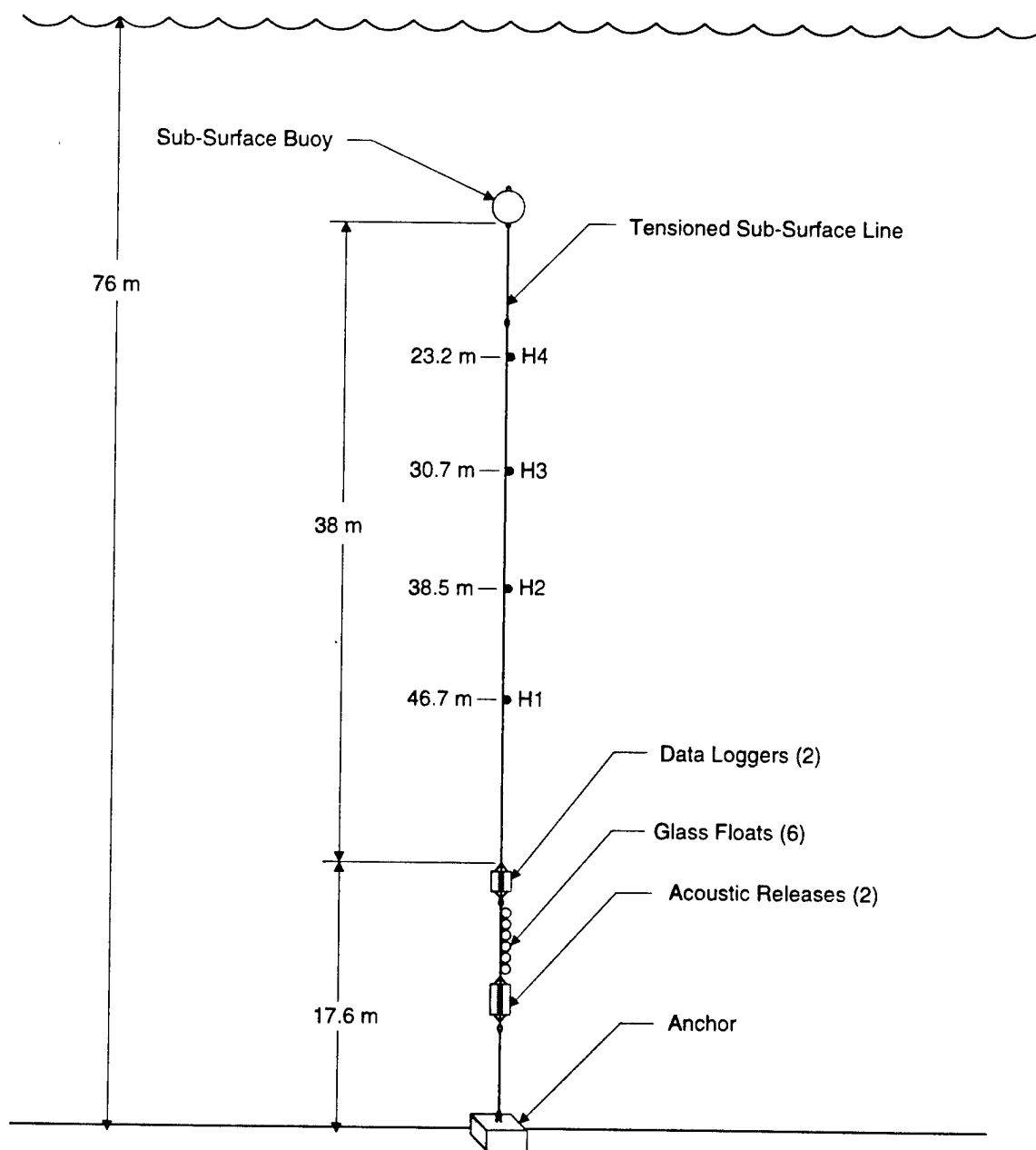
Anchor

Figure 19 Schematic layout of four-element, bottom-moored vertical array. Dimensions correspond to Deployment 2 (2200 on 29 August to 1100 on 31 August). The anchor consisted of links of steel chain (4-in. diameter) amounting to 375 kg of in-water weight, which gave the system a net negative buoyancy of approximately 200 kg.
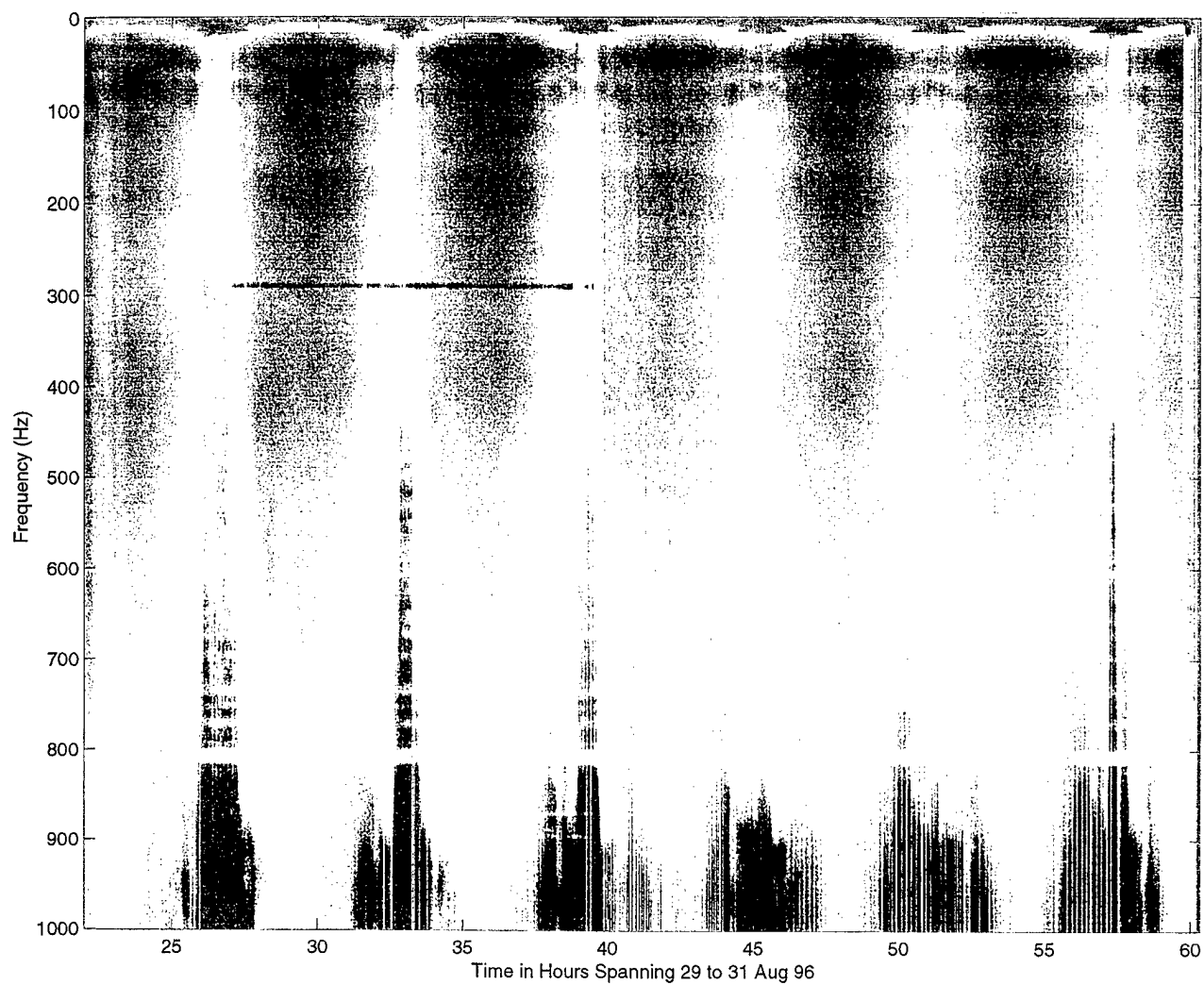
Figure 20. Spectrogram for the hydrophone element at depth 38.5 m.

Figure 21. Spectrogram for the hydrophone element at depth 46.7 m.

Figure 22. Time series of the original data demodulated by a 290-Hz tone (blue) and by a 300-Hz tone (red). Top corresponds to 38.5-m hydrophone depth (H2 of Figure 19); bottom corresponds to 46.7-m hydrophone (H1 of Figure 19).

decimated in a manner described by Dahl et al. [15], in order to arrive at a narrowband (baseband) signal with a total bandwidth of 0.5 Hz. The blue trace is the result of this processing when using 290 Hz as the demodulation frequency, and the red trace is the result when using 300 Hz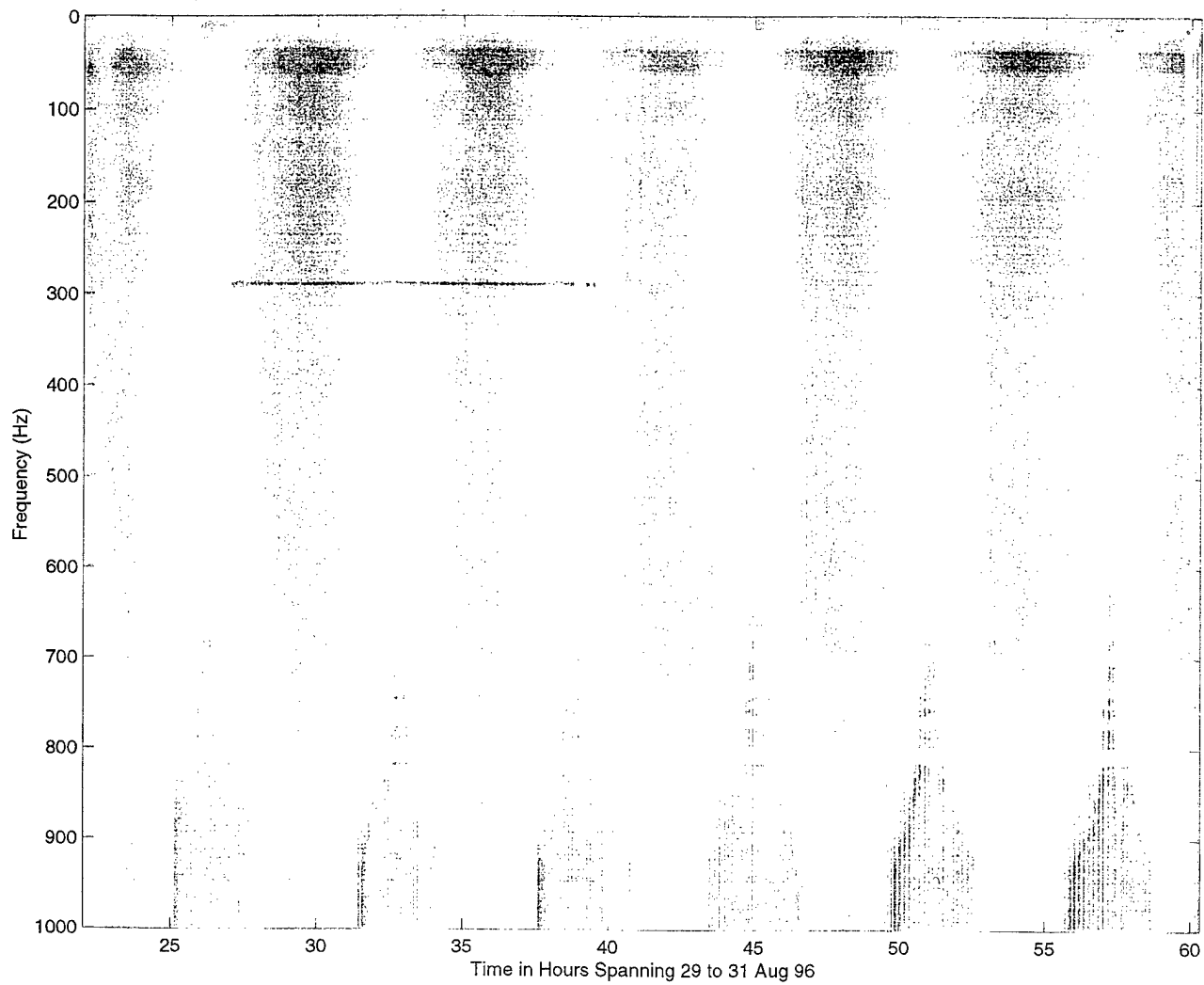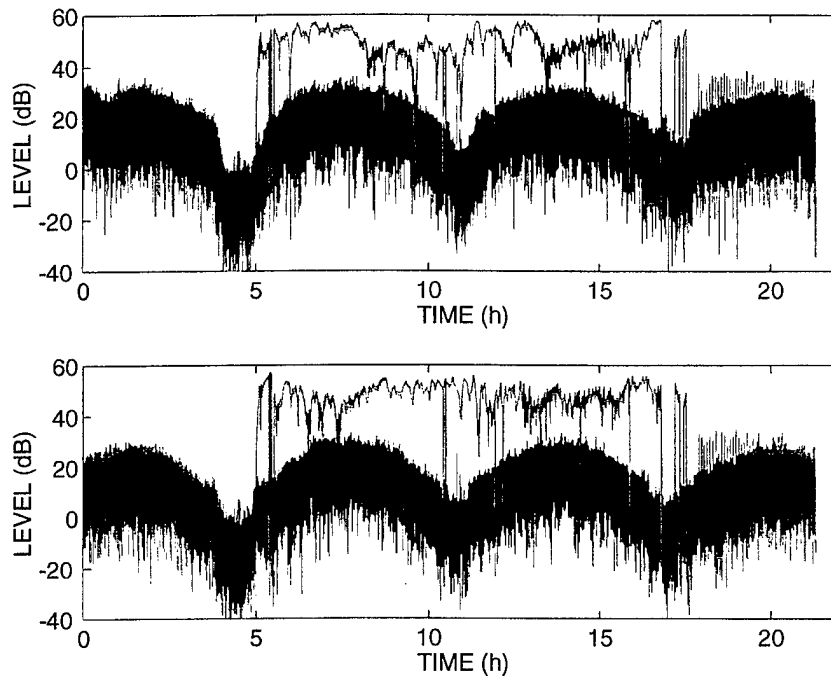 as the demodulation frequency (which we undertake for a clean estimate of the noise level in a nearby frequency band). The onset of the 290-Hz tone is clearly seen at hour 5, and the tone remains well above the noise for the 12-hour duration. (After the tone ceases, it commences again for about 20 min for reasons unknown.) The noise level recorded by both hydrophones differs by 25 to 30 dB between the longer-duration high-level periods and the shorter-duration low-level periods. The noise periodicity is best exemplified by the time between the low-noise events, with such events occurring about every 6 to 7 hours. The noise level for the 38-m hydrophone (top plot) is also about 3 dB greater than that for the 47-m hydrophone (bottom plot).

The variance of normalized intensity, or scintillation index, is defined as

$$S_I^2 = \frac{\langle I^2 \rangle}{\langle I \rangle^2} - 1, \tag{4}$$

where I is the acoustic intensity and the brackets denote time averaging. For the 12-hour period, $S_I^2 \approx 1$ for the upper hydrophone and $S_I^2 \approx 0.7$ for the lower hydrophone. We shall not at this stage interpret further these S_I^2 estimates, other than to say that we would anticipate the higher value for the upper hydrophone, as it lies closer to the thermocline boundary, which is undergoing vertical oscillation in addition to fluctuations likely associated with soliton activity.

Engineers from GTech also attached three autonomous-recording temperature sensors to this array at depths of 27 m, 33 m, and 39 m. Figure 23 shows the spectra of intensity fluctuations for both hydrophones, plotted along with temperature fluctuation spectra. (The thermistor data have been kindly provided by GTech.) The intensity fluctuation spectra are more or less similar with the exception of the spectrum for the shallower hydrophone, which shows a small, broad peak centered about 0.025 Hz (or 40 s), which is marked by the triangle. Unfortunately, we cannot find an equivalent peak in the temperature data, as they were sampled only every 30 s, so the highest frequency in the temperature fluctuation spectrum is 0.0167 Hz. Spectra associated with the temperature data do increase markedly in overall level
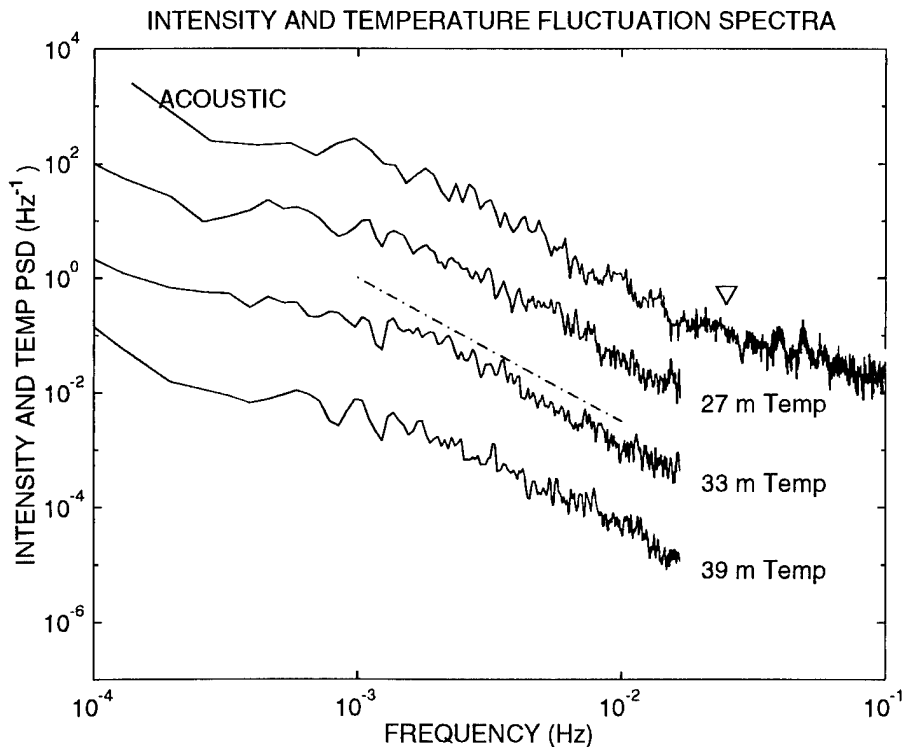
Figure 23. Acoustic intensity and temperature fluctuation spectra. The intensity data are the 12 hours of 290-Hz data shown in Figure 22. The black curve corresponds to the 46.7-m hydrophone, and the yellow curve corresponds to the 38.5-m hydrophone. The triangle above the yellow curve denotes 0.025 Hz. Depths for the three temperature fluctuation spectra are noted on the right of each curve, and the dashed line corresponds to a $f^{-2.5}$ decay.

as the thermistor depth decreases and approaches the thermocline. For frequencies less than about 10^{-2} Hz, all spectra follow roughly the same decay, and within the decade 10^{-3} to 10^{-2} Hz this decay is about $f^{-2.5}$, as indicated by the dashed line.

These are just a few glimpses of a potentially extraordinary database, with the results illustrated in Figures 20–23 posing more questions than providing answers. In future work we will seek to answer these questions.

6. SUMMARY

APL-UW fielded a 16-element vertical line array (VLA), which was suspended from the primary research vessel *Shi Yan 3*, and a four-element vertical array, which was deployed in a remote mooring, for the joint U.S.–China Yellow Sea Experiment.

Measurements of acoustic propagation using explosive TNT sources were made with the VLA. These measurements were reduced to *calibrated* estimates of transmission loss (to be distinguished from a more simple *relative* estimate of transmission loss), in third-octave frequency bands spanning the decade 80 to 800 Hz. To obtain calibrated estimates, we constructed a model for the source waveform and level for an explosive source, using equations available in the technical literature. We also deduced from the recorded waveforms that the preset denotation depth for TNT charges (given to us as 50 m) was off by 10 m on average. We included this effect in our estimation of transmission loss. However, all evidence to date suggests this error is not being included by others who have analyzed recordings made from the same explosive sources (e.g., c.f. Refs. 6 and 7).

A geoacoustic model for the seabed of the Yellow Sea was inferred from the data, using a combination of three methods: the analysis of headwave arrival times, the comparison of measured vs synthetic waveforms, and the comparison of estimated and modeled transmission loss values. We view this model to be a provisional one, as further analysis (see below) may lead to some modification. The geoacoustic model consists of a 2-m-thick sediment layer with a sound speed of 1555 m/s and an attenuation of 0.2 dB/λ, where λ is the acoustic wavelength, that separates the water from a basement halfspace with a sound speed of 1700 m/s and an attenuation of 0.07 dB/λ. This model is illustrated in Figure 3.

The four-element vertical array deployed in a remote mooring recorded data continuously for 38 hours. Two of the recording channels failed, but the remaining two recorded an extraordinary time history during which the ambient noise level varied by as much as 30 dB over a period between 6 and 7 hours. This period appears to be associated with the M2, or principal lunar, tidal mode (being roughly half the M2 period). A 290-Hz cw tone was emitted from a source suspended from the *Shi Yan 3* for 12 of the 38 hours. The subsequent recordings yielded valuable information on the nature of intensity fluctuations in the Yellow Sea. Temperature was also recorded on this mooring at three locations separated vertically. Spectra of both the intensity and temperature fluctuations assume a similar power-law decay of frequency to the minus 2.5 power.

This data set has posed many new questions, the answers to which will yield a valuable payoff in terms of understanding the nature of acoustic propagation in the Yellow Sea. In terms of further analysis we recommend the following lines of inquiry:

1. Is the small variation in transmission loss vs depth seen in the data a real effect of the seabed or an artifact of small variations in the hydrophone receive sensitivity? Filtering the data into much narrower bands (rather than using the present approach, which involved conventional third-octave bands) may resolve this question.

2. The energy spectrum for the headwave arrival (Figure 16) is remarkably narrow. What additional features of the seabed can be learned by modeling the spectral peak and bandwidth of this spectrum? Can additional headwaves, perhaps originating from deeper layers, be found in the data?

3. What is the source of the profound changes in ambient noise level (on the order of 30 dB), and can this change be predicted? Is this a unique feature of the Yellow Sea during summer conditions?

4. Can the nature of the ambient noise be understood by examining the correlation between the two vertically separated hydrophones on the remotely deployed array?

5. Can fluctuations in intensity as measured by the the remotely deployed array by modeled using Parabolic Wave Equation (PE) numerical propagation codes? Can the probability density function for intensity be modeled?

7. REFERENCES

1. P.H. Dahl and R.D. Light, Cruise Report on the Activities of the University of Washington Applied Physics Laboratory During the U.S.–China Yellow Sea Experiment, APL-UW TM 9-96, Applied Physics Laboratory, University of Washington, September 1996.

2. P. H. Dahl, R. C. Spindel, R. Odom, D. Tang, J. Zhou, P. H. Rogers, R. Zhang, and G. W. Caille, "Preliminary analysis of acoustic propagation data taken in the Yellow Sea," in *Shallow Water Acoustics*, R. Zhang and J. Zhou, Eds., China Ocean Press, 29–34, 1997.

3. J.-X. Zhou, "Normal mode measurements and remote sensing of sea-bottom sound velocity and attenuation in shallow water," *J. Acoust. Soc. Am.*, **78**(3), 1003–1010, 1985.

4. J.-X. Zhou, X. Zhang, and P. H. Rogers, "Effect of frequency dependence of sea-bottom attenuation on the optimum frequency for acoustic propagation in shallow water," *J. Acoust. Soc. Am.*, **82**(1), 287–292, 1987.

5. J.-X. Zhou, X. Zhang, P. H. Rogers, and J. Jarzynski, "Geoacoustic parameters in a stratified sea bottom from shallow water acoustic propagation," *J. Acoust. Soc. Am.*, **82**(6), 2068–2074, 1987.

6. S. Zhou, R. Zhang, L. Hao, L. Xiao, Y. Zheng and X. Tau, "Simulated annealing inversion for sea-bottom properties in the midst of the Yellow Sea," in *Shallow Water Acoustics*, R. Zhang and J. Zhou, Eds., China Ocean Press, 173–178, 1997.

7. L. Guo, R. Zhang, F. Li, W. Luo, X. Tau, and T. Zhou, "Inversion for sea bottom acoustic parameters using measured modal group time delays," in *Shallow Water Acoustics*, R. Zhang and J. Zhou, Eds., China Ocean Press, 179–184, 1997.

8. F. Li and R. Zhang, "Geoacoustic parameter inversion from waveform structure," in *Proc. 16th Int. Congress on Acoustics and 135th Meeting Acoustical Society of America*, 1619–1620, 1989.

9. N. Ross Chapman, "Measurement of the waveform parameters of shallow explosive charges," *J. Acoust. Soc. Am.*, **78**(2), 672–681, 1985.

10. J. Wakely, Jr., "Pressure-signature model for an underwater explosive charge," *U.S. Navy J. Underwater Acoustics*, **27**(2), 445–449, 1977.

11. F. B. Jensen and M. C. Ferla, SNAP: The SACLANTCEN Normal-Mode Acoustic Propagation Model, Report SM-121, SACLANT Undersea Research Centre, La Spezia, Italy, 1979.

12. G. V. Frisk, *Ocean and Seabed Acoustics: A Theory of Wave Propagation*, Prentice Hall, Englewood Cliffs, NJ, 1994.

13. M. B. Porter, The KRAKEN Normal Mode Program, Report SM-245, SACLANT Undersea Research Centre, La Spezia, Italy, 1991.

14. F. B. Jensen and W. A. Kuperman, "Optimum frequency of propagation in shallow water environments" *J. Acoust. Soc. Am.,* **73**(3), 812–819, 1983.

15. P. H. Dahl, A. B. Baggeroer, P. N. Mikhalevsky, and I. Dyer, "Measurement of the temporal fluctuations of cw tones propagated in the marginal ice zone" *J. Acoust. Soc. Am.,* **83**(6), 2175–2179, 1988.

REPORT DOCUMENTATION PAGE

Public reporting burden for this collection of information is estimated to average 1 hour per response, including the time for reviewing instructions, searching existing data sources, gathering and maintaining the data needed, and reviewing the collection of information. Send comments regarding this burden estimate or any other aspect of this collection of information, including suggestions for reducing this burden, to Washington Headquarters Services, Directorate for Information Operations and Reports, 1215 Jefferson Davis Highway, Suite 1204, Arlington, VA 22202-4302, and to the Office of Information and Regulatory Affairs, Office of Management and Budget, Washington, DC 20503.

1. AGENCY USE ONLY *(Leave blank)*	2. REPORT DATE December 1998	3. REPORT TYPE AND DATES COVERED Technical

4. TITLE AND SUBTITLE

Low-Frequency Sound Propagation in the Yellow Sea
Results from the 1996 China-U.S. Experiment

5. FUNDING NUMBERS

Contract N00014-96-1-1225

6. AUTHOR(S)

P.H. Dahl, C.J. Eggen, D.J. Tang, and R.C. Spindel

7. PERFORMING ORGANIZATION NAME(S) AND ADDRESS(ES)

Applied Physics Laboratory
University of Washington
1013 NE 40th Street
Seattle, WA 98105-6698

8. PERFORMING ORGANIZATION REPORT NUMBER

APL-UW TR 9804

9. SPONSORING / MONITORING AGENCY NAME(S) AND ADDRESS(ES)

Office of Naval Research
800 North Quincy Street
Arlington, VA 22217

10. SPONSORING / MONITORING AGENCY REPORT NUMBER

11. SUPPLEMENTARY NOTES

12a. DISTRIBUTION / AVAILABILITY STATEMENT

Approved for public release; distribution is unlimited.

12b. DISTRIBUTION CODE

13. ABSTRACT *(Maximum 200 words)*

Two sets of acoustic measurements made by the Applied Physics Laboratory, University of Washington, as part of the August 1996 joint U.S.–China Yellow Sea Experiment are analyzed. One set consists of broadband propagation measurements for which explosive TNT sources were used. These data were reduced to estimates of calibrated transmission loss, which, along with the recorded signal waveforms, were interpreted to infer a geoacoustic model for the seabed. The other set consists of narrowband acoustic fluctuation measurements plus broadband ambient noise measurements. The data show an extraordinary time history during which the ambient noise level varies by as much as 30 dB over a period of 6 to 7 hours.

14. SUBJECT TERMS

Yellow Sea, transmission loss, headwaves, intensity fluctuations, ambient noise

15. NUMBER OF PAGES

43

16. PRICE CODE

17. SECURITY CLASSIFICATION OF REPORT Unclassified	18. SECURITY CLASSIFICATION OF THIS PAGE Unclassified	19. SECURITY CLASSIFICATION OF ABSTRACT Unclassified	20. LIMITATION OF ABSTRACT SAR